Helsinki University of Technology
Department of Electrical and Communications Engineering
Espoo 2002

# Dispersion measurements of fiber-optic components and applications of a novel tunable filter for optical communications

Tapio Niemi

Dissertation for the degree of Doctor of Technology to be presented with due permission for public examination and debate in auditorium S4 at Helsinki University of Technology (Espoo, Finland) on the 14th of June, 2002, at 12 o'clock noon.

Helsinki University of Technology
Department of Electrical and Communications Engineering
Metrology Research Institute

Teknillinen korkeakoulu
Sähkö- ja tietoliikennetekniikan osasto
Mittaustekniikan laboratorio

Helsinki University of Technology
Metrology Research Institute
PL 3000
FIN-02015 HUT
Finland

Tel. +358 9 451 1
Fax. +358 9 451 2222
E-mail: **Tapio.Niemi@hut.fi**

ISBN 951-22-5986-9 (Electronic version)

ISBN 951-22-5985-0 (Printed version)
Picaset Oy
Helsinki 2002

**Abstract**

Optical communications has experienced a rapid development during the last decade. More bandwidth can be acquired by decreasing the spacing of the optical channels or by increasing the data rate. Characterization of the optical components and active monitoring of the network calls for accurate measurement methods. The objective of this thesis is to investigate and develop measurement methods and instruments for measuring important parameters of the components used in optical communications.

Chromatic dispersion of optical fibers and frequency chirp of the laser transmitters set limits for the data rate and transmission distance. Measurements of dispersion have traditionally been performed using a phase-shift method. When high modulation frequencies are applied to achieve high resolution an error could be introduced. In this thesis, the measurement accuracy of this method is analyzed in detail and a novel method for estimating the accuracy and correcting the measurement result is developed.

A Fabry-Perot interferometer finds numerous applications in many fields of optics. In this thesis, tunable Fabry-Perot etalon filters made of silicon were developed and several applications for these devices are demonstrated. A new device for measurements of time-resolved frequency chirp of directly modulated laser diodes in real time is developed. Interaction between the dispersion and frequency chirp limits the use of directly modulated lasers in long-haul optical links.

Another application is monitoring of the wavelength of optical transmitters. The wavelength of the laser diode may shift due to aging and active monitoring and controlling of the wavelength is required. In addition, the filter improves the performance of the directly modulated transmitter by temporal reshaping of the pulses. The filter is also applied in reducing the frequency chirp of gain-switched pulses generated with a diode laser. These pulses can then be made transform limited and can for example be used in generation of optical solitons.

Finally, the etalon is employed in realization of a compact wavelength reference for calibration of the wavelength scale of the optical spectrum analyzers and wavemeters. The transmission spectrum of the etalon consists of equidistant fringes. Each of these fringes can be applied as an accurate reference over a large wavelength range once the temperature of the filter is stabilized. This reference was developed to be automatic and it has an adequate accuracy for performing calibrations of field instruments.

Keywords: Wavelength division multiplexing, optical communications, fiber-optic components, dispersion measurements, Fabry-Perot etalon, tunable optical filters

**Preface**

The research work for this thesis has been carried out in the Fiber-Optics Group at the Metrology Research Institute of Helsinki University of Technology (HUT) during the years 1997-2002.

I would like to thank several persons who have made it possible to complete the thesis. Professor Pekka Wallin, the head of Department of Electrical and Communications Engineering and Prof. Erkki Ikonen for support and for an opportunity to work in the laboratory.

The supervisor of the work Docent Hanne Ludvigsen I would like to express my gratitude for introducing me to the field of optical communications and her tireless guidance especially during long writing periods. Simo Tammela of Technical Research Centre of Finland (VTT) has provided more ideas than anyone else and shared his long experience in many problems. Mikko Söderlund and Päivi Heimala of VTT have given a significant contribution in designing of electronics and manufacturing of the optical filters.

Maria Uusimaa and Goëry Genty have worked in several projects with me during these years providing invaluable help. I would also like to thank Dr. Jian-Guo Zhang for an interesting work on gain-switching.

Professor Matti Kaivola and Dr. Timo Kajava I acknowledge for their advice in preparation of the manuscripts.

Numerous people of Nokia Networks, Nokia Research Center and Teleste Ltd. have generously loaned equipment and shared their knowledge of practical aspects of optical communications.

Discussions with Dr. Mikko Merimaa have often softened the hard work and provided help in technical problems. Jesse Tuominen has made a good job in building electronics.

Funding of this work has been provided by Graduate School on Electronics, Telecommunications and Automation (GETA), Academy of Finland, National Technology Agency (TEKES) through the ETX-technology program, Centre for Metrology and Accreditation (MIKES), Jenny and Antti Wihuri Foundation and Tekniikan edistämissäätiö.

Finally, thank you Jaana-Piia for being loving, patient and supportive.

Tapio Niemi
Espoo, May 2002

**List of Publications**


[P1] T. Niemi, M. Uusimaa, and H. Ludvigsen "Limitations of phase-shift method in measuring dense group delay ripple of fiber Bragg gratings", *IEEE Photonics Technology Letters,* Vol. 13, pp. 1334-1336, 2001.

[P2] G. Genty, T. Niemi, and H. Ludvigsen "New method to improve the accuracy of group-delay measurements using the phase-shift technique", *Optics Communications,* Vol. 204, pp. 119-126, 2002.

[P3] T. Niemi, S. Tammela, T. Kajava, M. Kaivola, and H. Ludvigsen, "Temperature-tunable silicon-wafer etalon for frequency chirp measurements", *Microwave and Optical Technology Letters,* Vol. 20, pp. 190-192, 1999.

[P4] T. Niemi, S. Tammela, and H. Ludvigsen, "Device for frequency chirp measurements of optical transmitters in real time", *Review of Scientific Instruments,* Vol. 73, pp. 1103-1107, 2002.

[P5] T. Niemi, J-G. Zhang, and H. Ludvigsen "Effect of optical filtering on pulses generated with a gain-switched DFB laser", *Optics Communications,* Vol. 192, pp. 339-345, 2001.

[P6] T. Niemi, M. Uusimaa, S. Tammela, P. Heimala, T. Kajava, M. Kaivola, and H. Ludvigsen, "Tunable silicon etalon for simultaneous spectral filtering and wavelength monitoring of a DWDM transmitter", *IEEE Photonics Technology Letters,* Vol. 13, pp. 58-60, 2001.

**Author's Contribution**

The results presented in this thesis are a result of teamwork within the research group and co-operation projects with industry. The author has prepared the manuscripts of publications P1, P3-P5 and partly prepared the manuscript of publication P2 and P6.

For publication P1, the author developed the theoretical model and performed the numerical simulations. He also constructed the measurement setup and analyzed the measurement results.

For publication P2, the author developed the theoretical model and constructed the measurement setup. He also made the numerical simulations and analysis of the thin-film filter.

For publication P3, mainly the author designed and built the chirp analyzer. The measurements were carried out by him.

For publication P4, the author designed the electronics and constructed a prototype of the real-time chirp analyzer. He also performed the chirp measurements.

For publication P5, the author constructed the measurement setups and conducted all of the measurements and simulations.

For publication P6, mainly the author designed the electronics and the measurement setups. He participated in all the measurements.

The results reported in this thesis have also been presented in several international conferences.

## Table of contents

## 1 Introduction

The need for high-speed data transmission has enhanced the use of optical communication systems, which have experienced a rapid evolution during the last decade. New system concepts including dense wavelength division multiplexing (DWDM) and optical time division multiplexing (OTDM) have multiplied the transmission capacity of an optical fiber. Especially WDM provides a straightforward way to upgrade the capacity of the existing fiber lines. Optical transport networks are currently operating with bit-rates of 2.5 Gb/s or 10 Gb/s for each wavelength channel. The record breaking experiment in a single-fiber is at a rate of 10.9 Tbit/s for WDM transmission having 273 wavelength channels each carrying data at a rate of 40 Gbit/s over 117 km [1]. However, due to rapid development of new components this record will likely be broken in the near future.

The limitations in the quality of the signal are mainly set by the dispersion, nonlinearity and polarization-dependent effects of the optical fiber along with frequency chirping of the optical transmitters. The spacing of the DWDM-channels is defined to be a multiple of 100 GHz but components to realize channel spacing of 50 GHz are already available and feasibility of 25 GHz spacing is currently explored. Due to the decreasing channel spacing the characteristics of the components need to be carefully evaluated for optimization of the performance of the optical networks.

Dispersion of an optical fiber is one of the main limitations on the bit rate and length of the fiber within the optical communications systems. In modern networks, the signals pass through a number of components such as filters, multiplexers and switches. These components increase the amount of total dispersion. Therefore, it is important to characterize each component starting already at the manufacturing stage. The dispersion of optical components could be a problem especially in metropolitan area networks where a large number of these components are used in cascade. Dispersion is particularly harmful if the optical transmitter exhibits frequency chirp. Their interplay usually distorts the signal and degrades the performance of the network. Characterization of chirp of the optical transmitters can provide useful information for dispersion management and system simulations. Frequency chirp is mainly a problem in directly modulated laser diodes, which are currently the best solution for implementation of a cost-efficient optical transmitter. The effects of frequency chirp and dispersion can be counteracted by utilizing dispersion compensation or by using externally modulated transmitters. Both of these solutions will increase the cost of the system. On the other hand, directly modulated transmitters can be applied if their modulation properties are enhanced.

A conventional way of controlling the wavelength of a diode laser is to stabilize its temperature. A method to actively monitor and control of the wavelengths is required due to decreasing channel spacing and wavelength drift with aging of the diode lasers. An active research is going on to find an efficient and low-cost solution for this purpose. The wavelength of lasers can be accurately measured with wavemeters and optical spectrum analyzers. Although they are too bulky and expensive to be applied in on-line monitoring of the DWDM-channels they are invaluable instruments for accurate testing and measurement. To maintain the accuracy these devices, periodical calibration against a high-accuracy reference is needed.

### 1.1 Aims of the thesis

The thesis is divided into two themes. The first one deals with measurement of chromatic dispersion of various fiber-optic components. The second presents several applications of two novel optical filters.

The so-called phase-shift technique commonly applied to measure chromatic dispersion of optical fibers is investigated. It can also be used to measure the group delay of various components such as optical filters. The dispersion is obtained by differentiation of the group delay with wavelength. The results are reliable if the group delay varies smoothly over the wavelengths. To apply the phase-shift technique for measurements of various components whose group delay exhibit a strong variation with wavelength, it is important to be able to estimate the measurement accuracy. In this thesis, the accuracy of the technique is investigated theoretically and experimentally. Moreover, a new method to improve the accuracy is developed.

Furthermore, a novel temperature-tunable filter concept is introduced. The filter is based on a Fabry-Perot etalon with silicon as the cavity material. The refractive index of silicon has a strong temperature dependence, which allows a convenient tuning mechanism. A new device for measurements of time-resolved frequency chirp of directly modulated transmitters is developed based on the tunable filter. The chirp analyzer is further developed to operate in real time, which allows for continuous monitoring of the effects when the parameters of the laser diode are varied.

Another design of the temperature-tunable filter was manufactured. By placing this filter directly after the laser transmitter, simultaneous spectral filtering and accurate wavelength monitoring are demonstrated in an experimental link. The performance of the directly modulated laser in long-haul transmission is shown to improve if its spectrum is suitably filtered.

Generation of short optical pulses for high-speed optical communications is an active research topic. One way of generating short optical pulses from a diode laser is gain-switching. The gain-switched pulses exhibit large frequency chirp, which needs to be suppressed to permit utilization of these pulses in formation of optical solitons. Suppression can be accomplished by spectral filtering with the presented filter. However, the filtering causes the shape of the pulses to be distorted. This distortion was investigated both theoretically and experimentally.

The requirement for accurate measurements of the wavelength is set by the increasing density of channels in optical communication systems. The instruments applied to measure the wavelength need continuous maintenance to meet the accuracy specifications of long-term use. Therefore, their wavelength scale should be calibrated periodically. To perform these calibrations, a wavelength reference is being developed. It will primarily find use as a reference artifact for calibration of field instruments such as wavemeters and optical spectrum analyzers. The wavelength reference is based on the utilization of periodic transmission spectrum of a Fabry-Perot etalon. The transmission spectrum is accurately tuned and stabilized against environmental perturbations by applying temperature sensing and tuning.

# 2 Chromatic dispersion

The velocity of light is constant and independent of the wavelength in vacuum, whereas in materials it may vary with the wavelength of light. This phenomenon is commonly referred to as dispersion. The dispersion of optical components is due to a change in the index of refraction of the material used to build them with wavelength. In addition, reflections and interference effects inside the component can result in so-called geometrical dispersion.

## 2.1 Material dispersion

The refractive index of several materials, such as glass or various semiconductor materials is often modeled as a large number of harmonic oscillators [2]. The oscillators are the ions, molecules or electrons of the atoms. The electric field of light acts as a force, which pushes the particles into forced oscillation. The particles exhibit some characteristic resonance frequencies and they absorb energy from the driving electric field. This approach of modeling the material leads to the presentation of the refractive index of the material, which is often referred to as the Sellmeier approximation [2,3]. The refractive index of a variety of materials can be expressed as a sum of the characteristic resonant frequencies as

$$h^2 - A_0 = \sum_{j=1}^{m} \frac{A_j w_j^2}{w_j^2 - w^2} = \sum_{j=1}^{m} \frac{A_j l^2}{l^2 - l_j^2}, \tag{1}$$

where $h$ is the index of refraction, $A_j$ is the magnitude, $w_j$ is the angular frequency and $l$ is the wavelength of the $j$:th resonance. The parameter $A_0$ is a constant whose value is typically 1. Using this approximation the refractive index as a function of wavelength is often presented as a fractional polynomial having an order of three or five. Another approximation used to describe the refractive index of materials as semiconductors, is the Herzberger formula which can be written up to fourth order as [4]

$$\begin{aligned} h &= A + BL + CL^2 + D l^2 + E l^4 \\ L &= 1/(l^2 - 0.028) \end{aligned}, \tag{2}$$

where $A$, $B$, $C$, $D$, and $E$ are coefficients obtained from a fit to the measured data. The wavelength $l$ is given in micrometers in Eq. (1) and Eq. (2). The coefficient $L$ and the value 0.028 are included to take into account the rapid rise in the index of several semiconductor materials at short wavelengths.

The index of refraction defines the velocity of light within the medium according to the relation $c=c_0/h$, where $c_0$ is the velocity of light in vacuum. This velocity is also referred to as phase velocity, which indicates the velocity of the phase of monochromatic light. When information needs to be transmitted along the laser light, modulation of it is required. The modulation increases the bandwidth of the signal. The velocity of this signal through the system is called the group velocity and it is defined as $v_g=c_0/h_g$, where $h_g$ is a group index. The group index can be calculated using

$$h_g = h + w\frac{dh}{dw} = h - l\frac{dh}{dl}. \tag{3}$$

If the material is not dispersive, i.e. the derivative of the refractive index with optical frequency is zero, the phase and the group velocities are equal. When the group velocity is

smaller than the phase velocity, the material is defined to exhibit normal dispersion. In this case, light with a lower frequency travels faster than light with a higher frequency. In the opposite situation, the material is defined to exhibit anomalous dispersion. An optical fiber fabricated of fused silica ($SiO_2$) has both normal and anomalous dispersion depending on the wavelength. The material of the core of the optical fiber is silica slightly doped to form a waveguide by increasing the refractive index. The dispersion of the material is often defined by the dispersion parameter $D$. It can be calculated using the second derivative of the refractive index as

$$D = -\frac{l}{c_0}\frac{d^2h}{dl^2}, \tag{4}$$

where $c_0$ is the speed of light in vacuum. The refractive index of silica has been determined by fitting the measured data to the Sellmeier equation. The coefficients of the equation are $A_1$=0.6961663, $A_2$=0.4079426, $A_3$=0.8974794, $l_1$=0.0684043 $m$m, $l_2$=0.1162414 $m$m and $l_3$=9.896161 $m$m [3]. The refractive index and the group index of bulk silica glass are shown in Fig. 1a. It can be observed that the group index has a minimum value at a wavelength around 1300 nm. The dispersion $D$ is shown in Fig. 1b. This value drops to zero at around 1276 nm which is called zero dispersion wavelength. The silica glass exhibits normal dispersion below this value and anomalous dispersion at longer wavelengths.

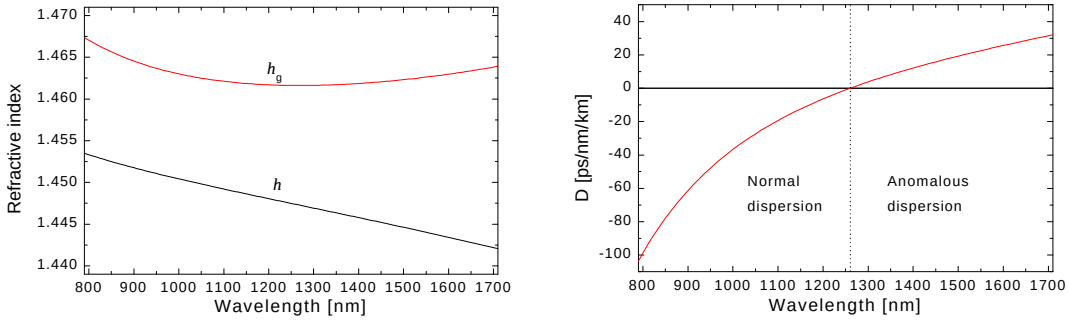


**Figure 1.** a) The refractive index and group index of bulk silica. b) Dispersion of bulk silica.

### 2.2 Tailoring of the dispersion

In addition to the material dispersion, the component may also have dispersion resulting from resonant absorption, reflections within a cavity or from waveguide effects. These dispersion effects are referred to as geometrically or structurally induced dispersion.

In an optical fiber, the dispersion is affected by the doping of the core and by waveguide dispersion. The waveguide dispersion shifts the zero dispersion wavelength of a standard single-mode fiber to slightly longer wavelengths, around a value of 1310 nm. Moreover, it can be applied to shift the dispersion to even longer wavelengths or to flattening of the dispersion. The interferometric dispersion of the component results from of a number of reflections within the structure forming an optical cavity. The output field of a cavity is composed of light fields, which have been reflected several times within the component. Since each of the beams has spent different time within the cavity, the output field effectively experiences a delay, which depends on the wavelength. The molecular absorption and optical cavities change the amplitude of the light passing through them [5]. In general, any component having a wavelength dependent loss or gain will also induce a change in the refractive index and hence introduce dispersion. The variation in the gain or loss of the component and the variation in the refractive index can be related to each other by the Kramers-Kronig relations. These relations are often referred to as a Hilbert transform. They

are in general valid for any component fulfilling the principles of causality [6]. The linear characteristics of the optical component can be completely defined by using a complex transfer function, which can be written as $H(w) = A(w)e^{jf(w)}$. Here $w$ is the optical angular frequency, $A$ is the amplitude response and $f$ is the phase response of the component. The complex transfer function can be calculated either analytically or numerically. If the transfer function is modified into the form $\ln H(w) = \ln A(w) + jf(w)$, the Kramers-Kronig relation for the phase and amplitude response can be written as [6]

$$f(w) = -\frac{w}{p} P \int_0^{\infty} \frac{\ln A(w)}{w'^2 - w^2} dw', \tag{5}$$

where $P$ indicates a principal value of the integral. This equation can be applied to calculate the phase response of the component from the measured amplitude response.

The parameter used to describe the dispersive time delay induced by the component for the signal is denoted group delay. The group delay, $t_g$, of the component is defined as a derivative of the phase response as

$$t_g = -\frac{d}{dw} f(w). \tag{6}$$

The dispersion parameter $D$ of the component is the derivative of the group delay with respect to wavelength

$$D = \frac{d}{dl} t_g. \tag{7}$$

As in the case of an optical fiber also components may exhibit regions of normal and anomalous dispersion due to structural effects. This fact is useful in designing components, which can be used to compensate for the dispersion of standard single-mode fibers. Such devices are typically optical filters whose group delay properties can be designed to have a desired dispersion profile.

### 2.3 Measurement methods for chromatic dispersion

The dispersion of optical components is an important parameter, which has a significant effect on the performance of various optical systems. Analysis and accurate measurement of the dispersion is therefore essential in optimization of the performance of such systems. Measurements of chromatic dispersion can be performed by applying various techniques. They include applications of Kramers-Kronig relations or a Hilbert transformation between the reflectivity and the phase of the components, low-coherence interferometry, and various pulse delay measurements and phase-shift techniques. The parameter that is typically measured is the group delay of the component as a function of the wavelength. Traditionally the dispersion of an optical fiber has been an important characteristic to be measured. In practice, it is important to have knowledge of such parameters as the zero-dispersion wavelength, the dispersion slope and uniformity of the dispersion of the manufactured fiber. Recently, the dispersion of optical components as optical filters has gained a lot of interest. In particular, the development of the filters based on fiber Bragg gratings (FBGs) permit for compensation of the dispersion of an optical fiber. By applying FBGs, the dispersion effects can be dramatically decreased in long-transmission systems. Accurate characterization of the dispersion of these filters requires evaluation of the conventional methods to obtain reliable measurement results of their properties.

*Measuring dispersion using Hilbert-transform method*

The amplitude and the phase response of an optical filter are related via the Hilbert transform. To assure this relation is valid, the filter must fulfil a so-called minimum phase condition [6,7]. It has been shown that this condition is fulfilled by a number of optical filters, such as uniform fiber Bragg gratings and symmetrical thin-film filters. For these components, the phase response and then the dispersion can be calculated directly from the measured amplitude response [8-10]. However, the minimum phase condition does not hold for component including various types of apodized or chirped fiber Bragg gratings and allpass filters as Gires-Tournois interferometer [6]. These components have a complex phase response and it has been shown that in general the reconstruction of the phase information from the measured amplitude response is not possible.

*Measuring dispersion using interferometric methods*

To obtain the group delay and the dispersion of the components interferometric methods or methods based on measuring the transmission time through the components are applied. In the interferometeric methods, the measurement setups are typically based on Michelson or Mach-Zehnder interferometers [6,11-16]. Light from a broadband or a wavelength tunable light source is split in two paths one of which couples light into the component and the other is a reference path. The light has transversing the component is combined with the light from the reference path and the resulting interferogram is detected. From this interferogram it is possible to calculate both the amplitude and the phase response of the component by means of a Fourier transform. The group delay of the component can be extracted from the phase of the interferogram. A clear advantage of the interferometric method is its resolution. Very small dispersion values can be measured accurately. However, interferometers often use free-space optics, which make them sensitive to variations in the environment. Also long components are difficult to be measured since the length of the reference arm needs to be approximately equal to the optical length of the device under measurement.

### 2.4 Conventional phase-shift technique

In applications with moderate requirements on the resolution, methods based on the transverse time of a modulated light are used. These methods include pulse-delay measurements and various phase-shift techniques [17-21]. A basic measurement setup for the phase-shift technique is outlined in Fig. 2. The light from a tunable laser is intensity modulated with a sinusoidal signal. The modulation generates sidebands on both sides of the optical carrier. The sidebands will experience a phase shift when the modulated light passes through the device under test. The phase shift of the detected signal allows the group delay of the component to be determined. The basic setup and variations of it using different light sources have been utilized for measurements of the dispersion of an optical fiber for years. Several commercially available dispersion measurement systems rely on this measurement principle [22-24].

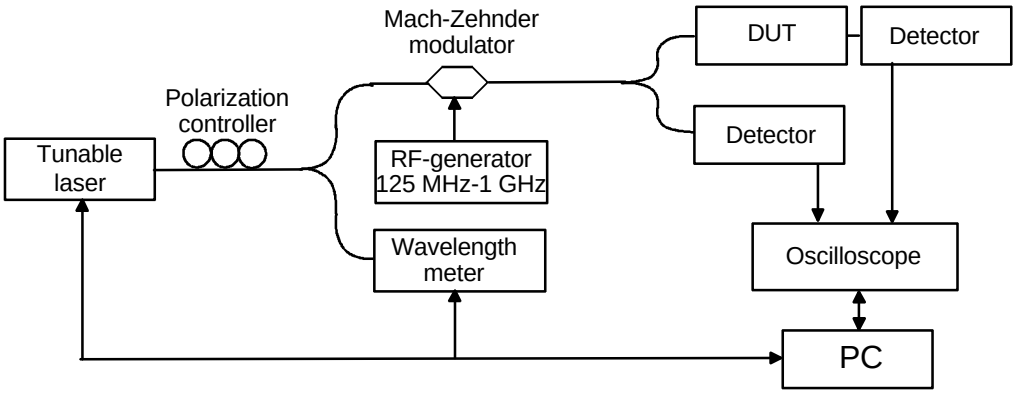


**Figure 2.** Experimental setup to measure dispersion using the phase-shift technique [P1,P2].

When the phase-shift method is employed for measuring group delay of an optical fiber whose group delay varies smoothly with wavelength, the measurement results are accurate. However, in components as for instance optical filters the group delay may exhibit large variation with wavelength. To be able to interpret the measurement results obtained with the phase-shift method, a model of the operation principles of this technique is derived. The electrical field of the sinusoidally modulated light can be presented as

$$E_{out} = \sqrt{P_0(1+m\cdot\cos(w_m t))}e^{jw_0 t} \approx \sqrt{P_0}(1+\frac{1}{2}\cdot m\cdot\cos(w_m t))e^{jw_0 t}, \tag{8}$$

where $w_0$ is the center optical frequency, $m$ is the intensity modulation index, $P_0$ is the average optical power and $w_m$ is the angular intensity modulation frequency. When the modulated light passes through the component having dispersion the sidebands will experience a phase shift compared to the center optical frequency. The detected photocurrent after the component can be written as

$$I \approx E_{out}E_{out}^{*} = P_0\left\{1+m\cdot\cos[w_m t+q(w_0)]\cdot\cos\left[\frac{1}{2}\left(f^{+}+f^{-}\right)\right]\right\},$$
$$q(w_0) = \frac{1}{2}(f^{+}-f^{-}) \tag{9a, 9b}$$

where $q(w_0)$ is the measured electrical phase shift and $f^{\pm}$ are the optical phase shifts of the two sidebands. The cosine term including the sum of the optical sidebands is usually omitted in derivation of the operation principles since it does not have any contribution to the measured electrical phase shift. However, this term induces fading of the amplitude of the detected intensity for certain combination of the dispersion and the modulation frequency [25].

The dispersion induced group delay is usually assumed to be constant in a narrow band around the optical carrier [18]. In this case, the phase shift for the two optical sidebands is given by

$$f^{+}-f^{-} = \int_{w-w_m}^{w+w_m} t_{comp}(x)dx = 2w_m t_{meas}(w), \tag{10}$$

where $t_{comp}(w_0)$ is the true group delay of the component and $t_{meas}(w_0)$ is a measurement result of the group delay of the component at the optical carrier frequency. This approximation leads to the well-known relation for the measured group delay

$$t_{meas}(w) = \frac{f^+ - f^-}{2w_m} = \frac{q(w)}{w_m}. \qquad (11)$$

It is evident from this expression that a higher modulation frequency allows for a higher resolution of the measured group delay. The resolution of the technique is technically limited by the device utilized for the measurement of the electrical phase. Typically these devices are network analyzers, vector voltmeters, lock-in amplifiers or oscilloscopes. All of these instruments have a limited resolution of the phase measurement. In Table 1 the resolution of the phase-shift method is given for different modulation frequencies and for different phase measurement resolutions.

***Table 1. Group delay resolution of the phase-shift method.***

| Modulation frequency [MHz] | Timing resolution for 0.1° [ps] | Timing resolution for 0.05° [ps] |
|---|---|---|
| 125 | 2.22 | 1.11 |
| 250 | 1.11 | 0.56 |
| 500 | 0.56 | 0.28 |
| 750 | 0.37 | 0.19 |
| 1 000 | 0.28 | 0.14 |

If the group delay exhibits large variation the operation of the phase-shift technique can be analyzed by constructing the group delay of the component utilizing its Fourier-components [P2]. This analysis leads to an instrument function that describes the measured group delay as a function of the actual group delay. This instrument function of the phase-shift method can be expressed as

$$t_{meas}(w) = \int_{-\infty}^{\infty} \tilde{t}_{comp}(u) \cdot \frac{\sin(w_m u)}{w_m u} \cdot e^{jwu} du = t_{comp}(w) * rect(w / 2w_m), \qquad (12)$$

where * denotes convolution operation. From this expression it is easy to identify the instrument function of the phase-shift method to be a rectangular function of width $2w_m$. This function can then be applied in analyzing the effects of the modulation frequency of the phase-shift technique to an arbitrary group delay. Moreover, it can be used to reconstruct the actual group delay $t_{comp}$ of the component which has been degraded by the measurement.

**2.5 Measurement results using phase-shift technique**

The phase-shift method can be utilized in measuring a variety of components ranging from optical fibers to optical filters. A component that has received a lot of attention lately is a dispersion-compensating fiber Bragg grating. This type of grating is fabricated to have a linear variation of the period of the index modulation of the grating part [26-28]. The variation in the period causes different optical frequencies to reflect at slightly different positions along the length of the grating. This introduces an effective delay between the different frequency components allowing tailorable dispersion properties for the grating. Although the basic idea of the dispersion compensating grating is quite simple it has turned out that manufacturing of such gratings having acceptable performance is a demanding process.

In this thesis, the phase-shift technique was used to investigate the dispersion of a dispersion-compensating grating. The measured reflectivity and the group delay of the grating are shown in Fig. 3a. The bandwidth of the 20 cm long grating is ~2 nm. The nominal dispersion was extracted by fitting a line in to the measured group delay. The dispersion of the component is $D$=-660 ps/nm which is sufficient for compensating the dispersion of 40 km of single-mode fiber. The group delay of the grating is nominally linear over the bandwidth of the grating. However, there are deviations from the linear group delay. This variation was measured in detail utilizing several modulation frequencies. The measurement of the group delay over a small wavelength portion is displayed in Fig. 3b. Each of the lines is an average of five distinct measurements. First, it can be observed that the variation is not random since it exhibits almost the same shape in repeated measurements with different modulation frequency. Secondly, the magnitude of the variation decreases when higher modulation frequencies are applied.

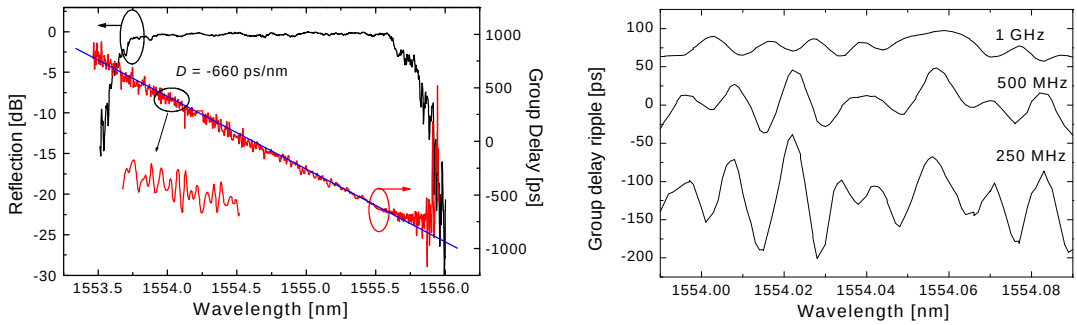


**Figure 3.** a) Reflectivity and group delay of a dispersion-compensating grating. b) Effect of the modulation frequency on the measured amplitude of the group delay ripple.

The variation of the group delay is referred to as group delay ripple and it is one of the main factors limiting the utilization of these gratings in real systems [29-32]. The ripple results from the imperfections during the manufacturing process and from the apodization profile of the refractive index modulation in the grating [33-35]. When the phase-shift method is used for characterization of the gratings, the selection of the modulation frequency will have a significant effect on the measurement result [30,36,P1].

### 2.6 New method for improving the measurement accuracy

The reason behind the decrease and inversion of the sign of the amplitude of the ripple can be found from the instrument function of the phase-shift method presented in Eq. (12). As a simple example, the analysis of the measurement result can be performed for sinusoidal ripple variation. When sinusoidal group delay ripple is analyzed utilizing the instrument function, it can be shown that the measured amplitude of the ripple will behave like a sinc-function

$$A(w_m) = A_p sinc(\frac{w_m}{p}), \qquad (13)$$

where $w_m$ is the angular modulation frequency and $A_p$ is the amplitude of the ripple [P1]. The important parameter in this equation is the ratio of the modulation frequency and the period of the ripple. It can be directly seen that the amplitude of the ripple having a period that is a multiple of a half of the modulation frequency will have zero measured amplitude. Also the measured amplitude of the ripple has decreased by 50 % if the modulation frequency is more than ~1/3 of the period of the ripple. Moreover, if the modulation frequency falls in the region from half of the ripple period to the full period, the amplitude of the ripple changes its

sign. This behavior was observed during the measurements with higher modulation frequencies and it can be seen in Fig. 3b when a modulation frequency of 1 GHz was used. Attempts to modify the conventional method have been proposed to improve the measurement accuracy even when higher modulation frequencies are applied [37]. However, this modified method requires an accurate means to control the wavelength and modulation frequency.

The instrument function allows the measurement accuracy of the phase-shift method to be conveniently explored by means of a Fourier-transformation as was demonstrated with sinusoidal delay ripple. However, the instrument function can also be applied to reconstruct the original group delay of the component from the measured group delay, which is degraded by the use of a high modulation frequency. The method is based on performing a de-convolution to the measured group delay. The de-convolution can be conveniently performed by applying a Fourier transform. In the Fourier domain, the operation can be made by simply dividing the measured group delay with the sinc-function. The actual group delay of the component $t_{comp}$ can then be written as

$$t_{comp}(w) = \Im^{-1}\left[\frac{\tilde{t}_{meas}(u)}{\mathrm{sinc}(w_m u)}\right]_w , \qquad (14)$$

where $\tilde{t}_{meas}(u)$ is the Fourier transform of the measured group delay and $\Im^{-1}$ designates the inverse Fourier transform. An example of the effect of the reconstruction for the group delay measured for chirped FBG and a narrow band thin-film filter are shown in Fig. 4. The group delay of the FBG was first measured with a high modulation frequency of 1 GHz. The reconstruction was then applied to the measured data. In Fig. 4a the reconstructed group delay is compared with the delay measured with a low modulation frequency of 250 MHz. This can be considered as the actual group delay of the component since all of its Fourier components occur well before the first zero of the sinc-function in Eq. (14) [P2]. A similar reconstruction was applied to the group delay of the thin-film filter. In this case, the transmission spectrum of the filter was calculated and the measurement setup was built within a simulation program *Gigabit Optical Link Designer* (GOLD) [38,P2]. The simulation was executed for a modulation frequency of 2 GHz, which was selected to match the modulation frequency of commercially available measurement systems. A decrease in the measured delay near the sharp peak is observed in Fig. 4b. After the reconstruction, the height of the peaks in the original group delay was restored.

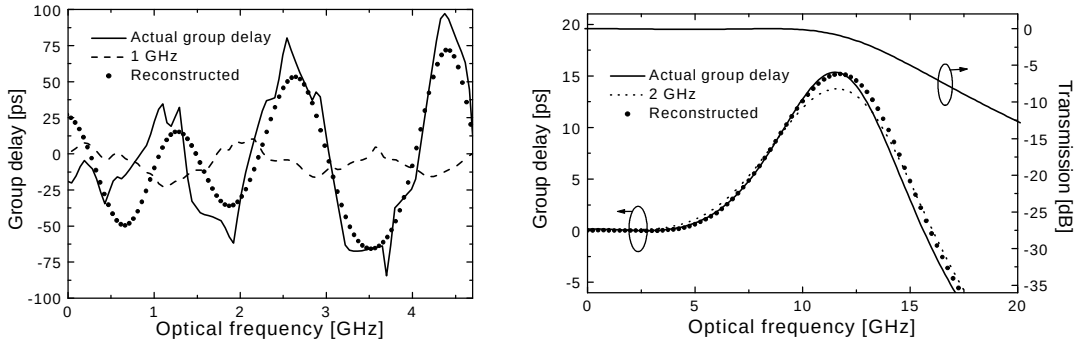


**Figure 4.** Measured and reconstructed group-delays of a) chirped FBG and b) narrow band thin-film filter [P2]. Only one half of the symmetrical transmission spectrum of the thin-film filter is displayed.

This new method permits an improvement of the accuracy of the conventional phase-shift technique without any modifications to the measurement setup. Important conditions for

successful reconstruction of arbitrary group delay profiles are that the Fourier components are below the zero points of the sinc-function and the wavelength step is small enough to resolve the ripple period. The reconstruction is done by post-processing of the measured group delay [39,P2].

## *APPLICATIONS OF A NOVEL TUNABLE FILTER*

# 3 Tunable filter based on Fabry-Perot etalon

Tunable optical filters find numerous applications in optical telecommunication systems. They can be configured to actively select optical channels in WDM systems or they can be used to monitor the optical wavelength of the channels. Tunability of the filters can be realized by heating or mechanical tuning of some of the parameters of the filter. Often the structure of the tunable filter device is based on a Fabry-Perot interferometer. A Fabry-Perot interferometer is a cavity with mirrors at both ends. The cavity can be simply air or filled with some transparent material, such as glass or semiconductor. Tuning of the bandwidth and the center wavelength of the passband of the filter can be realized either by modifying the reflectivity of the mirrors or tuning the optical thickness of the cavity. The tuning of the thickness can be realized for example by tilting, heating or by mechanically tuning the length of the cavity [40-44].

In this thesis, the tunable filters were Fabry-Perot etalons, which have silicon as the cavity material. Silicon is an attractive choice as cavity material since it has low absorption in the wavelengths of interest for optical telecommunications. Silicon wafers are standard products and widely used in the semiconductor industry. The methods for fabricating silicon-based components are also well developed which allows for potentially low-cost device implementation. The wavelength range at which silicon is transparent covers a wide range from 1.1 *m*m to 5 *m*m as can be observed from Fig. 5a [45]. The material absorption starts to increase rapidly when the wavelengths approach values below 1.2 *m*m, since these wavelengths are close to the band edge of silicon. The absorption starts to increase after the wavelength of 5 *m*m but the absorption remains at a sufficiently low level up to 40 *m*m. However, this data should not be considered to have absolute accuracy since it has been pointed out that the variation between different measurements give different values for absorption and also for the refractive index. Both of these quantities depend heavily on the purity and free carrier concentration of the silicon sample [46]. The refractive index of silicon is high which is typical for many semiconductor materials. The refractive index of silicon can be presented by the Herzberg-type formula presented in Eq. (2). Numerical values for the polynomial coefficients are $A$=3.41906, $B$=1.23172·10$^{-1}$, $C$=2.65456·10$^{-2}$, $D$=-2.66511·10$^{-8}$, and $E$=-5.45852·10$^{-14}$ [46,47]. The refractive index as a function of wavelength is presented in Fig. 5b.

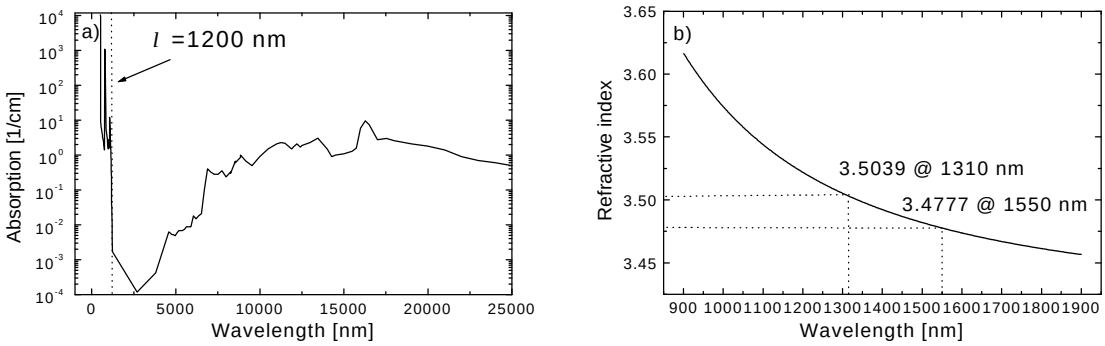


**Figure 5.** a) Absorption spectrum of silicon. b) Refractive index of silicon as a function of wavelength.

Due to the high index of refraction of silicon the polished wafer surface can operate as a mirror of the Fabry-Perot etalon even without any coating. The reflectivity of the silicon-air interface is ~ 0.3. The reflectivity of the silicon surfaces can be increased by depositing dielectric mirrors on both sides of the wafer. The mirrors can be formed by using a stack of quarter wavelength thick thin-film layers. Typical materials which can be applied for this purpose are $TiO_2$ ($h$=2.1), $Si_3N_4$ ($h$ =2.0) and $SiO_2$ ($h$ =1.45).

The transmission spectrum of the Fabry-Perot cavity can be calculated by summing up the electrical fields from multiple reflections within the filter cavity [48]. The result for the transmission for the electric field can be expressed in the optical frequency domain with a complex transfer function

$$T(w) = \frac{(1-R)\cdot e^{-jd/2}}{1-R\cdot e^{-jd}}, \tag{15}$$

where $R$ is the power reflectivity of the facets and $d$ is the phase shift of the optical field for one round trip within the cavity. The transmission spectrum of the etalon consists of periodic fringes. The center wavelength of the transmission fringe of the Fabry-Perot filter is located at a wavelength, which is multiple integer of half of the wavelength. The period of the transmission fringes is characterized by the free spectral range (*FSR*). The inverse of *FSR* presents time needed for the light to make one round trip within the cavity. The *FSR* can be defined as

$$FSR(q) = \frac{c_0}{2Lh\cos q}, \tag{16}$$

where $c_0$ is the speed of light in vacuum, $L$ is the length of the etalon cavity, $h$ is the refractive index and $q$ is the angle of the incident light with the surface normal. The *FSR* depends both on the wavelength and the temperature of the etalon if the angle of incidence is fixed.

The power transmission of the Fabry-Perot etalon can be calculated by taking a squared absolute value of the complex transfer function of Eq. (15). The complex transfer function indicates that the cavity has inherently some geometrical dispersion in addition to the material dispersion. The complex transmission function leads to the optical phase response of the etalon written as

$$f(w) = -\arctan\left(\frac{1+R}{1-R}\tan\frac{w}{2\cdot FSR}\right). \tag{17}$$

The group delay of the etalon in transmission can then be analytically calculated to be

$$t_g(w) = \frac{1}{2\cdot FSR}\frac{(1-R^2)}{1+R^2-2R\cos(\frac{w}{FSR})}. \tag{18}$$

The transmission and group delay of the etalon are displayed in Fig. 6 for two reflectivity values of $R$=0.6 (*solid line*) and $R$=0.8 (*dotted line*). For a Fabry-Perot etalon, the dispersion is normal at frequencies below the center frequency of the transmission fringe. On the other side of the transmission fringe, the dispersion is anomalous.

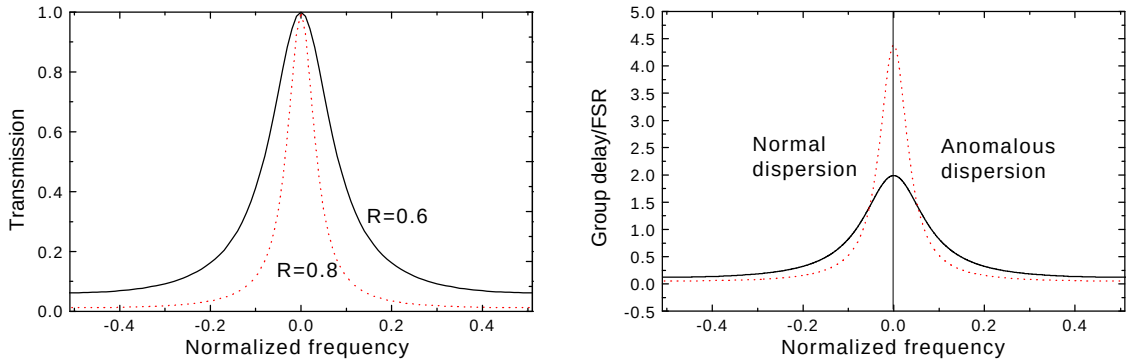


**Figure 6.** Transmission and group delay of a Fabry-Perot cavity. The group delay is normalized with the *FSR* of the cavity.

Similar kind of behavior can be observed for numerous optical filters such as multi-cavity thin-film filters and fiber Bragg gratings. For these structures, the group delay has a small variation within the center of the flat pass band and sharp peaks near the edges of the transmission or reflection band [44]. The deviation of the transmitter wavelength from the center of the filter passband may cause additional dispersion penalty [7]. On the other hand, the dispersion of the filters can be utilized in compensation of the dispersion of the optical fiber.

### 3.1 Temperature tuning of the Fabry-Perot etalon

The tuning of the center wavelength of the passband of the filter can be conveniently done with temperature. It results from the fact that the refractive index of silicon exhibits a strong temperature dependence at wavelengths near the absorption band edge of the material. A change in the temperature will shift the absorption edge, which induces a variation in the refractive index according to the Kramers-Kronig relations. Attempts to calculate the magnitude of the temperature dependence of the refractive index of silicon have been made [49]. However, the calculations have only explained the sign of the temperature coefficient and given an order of magnitude of its value. The temperature coefficient of refractive index of silicon has been measured to be ~$1.5 \cdot 10^{-4}$ 1/K [46,49]. In addition to the change in the refractive index, the changes in the temperature induce thermal expansion of the cavity. However, this effect is smaller by two orders of magnitude since the thermal expansion coefficient of silicon is $2.5 \cdot 10^{-6}$ 1/K. The shift of the center wavelength due to both of these effects can be calculated from

$$\frac{dn_0}{dT} = -n_0\left(\frac{1}{h}\frac{\partial h}{\partial T} + b\right), \tag{19}$$

where $n_0$ is the center frequency, $\partial h / \partial T$ is the temperature dependence of the refractive index and $b$ is the temperature expansion factor of the length of the cavity. For example, in the 1550 nm region a shift of the center wavelength of $dn_0/dT$=-8.8 GHz/K (70 pm/K) is expected.

Tuning and sensing of the temperature of the etalon filter was realized with two thin-film resistors integrated on its surface. One of the resistors is used to heat the chip. Heating is realized simply by feeding current through the resistor. The other resistor can be used to measure the changes of the temperature of the chip. The resistors are composed of molybdenum films to achieve good thermal contact with the silicon wafer. The thickness of the films is ~200 nm. The resistance values have slight variation among different filter chips,

but values between 900 Ω and 1.7 kΩ for the sensing resistor and ~35 Ω for the heating resistors have been measured. The resistors were deposited on the surface of the chip by sputtering. A photograph of the filter chip showing the heating and sensing resistors is displayed in Fig. 7a. Light passes through the filter at the center of the circular resistors. To connect the filter as a part of a fiber optic system the chip mounted on a piece of a circuit board and inserted in an air gap of a fiber-optic beam expander (Fig. 7b).

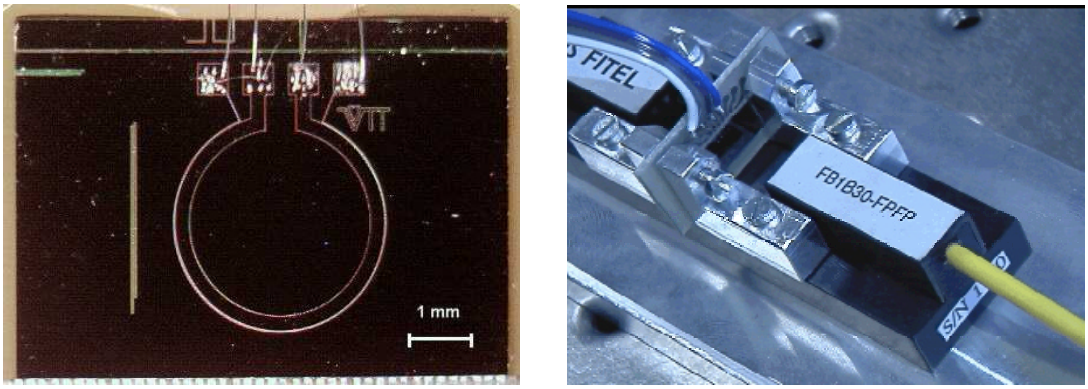


**Figure 7.** a) Photograph of the Fabry-Perot etalon based on silicon wafer [P4]. b) The etalon mounted in an air gap of a fiber-optic beam expander.

The sensitivity of the temperature tuning was determined by feeding current through the chip and measuring the temperature with a temperature sensor (LM45). The sensor was glued to the surface of the chip in the vicinity of the temperature sensing molybdenum resistor. The heating current was gradually tuned and the transmission of the filter was measured. From the transmission it was possible to calculate the sensitivity for the temperature tuning as ~11 GHz/K. This indicates a value of ~$1.85 \cdot 10^{-4}$ 1/K for the temperature coefficient. Which is close to values measured for temperature tunable etalons by other research groups [42,121] but different from the value measured with other techniques. The speed of the tuning of the chip depends on the applied heating power, the size of the silicon chip and on the initial temperature. In practice, all the filters have the same size of ~ 6 mm × 8 mm × 380 ㎜. For these chips, the speed of the heating was measured to be ~10 K/s (110 GHz/s). The dependence of the heating speed on the chip size was simulated by using a finite element method. A heating power of 100 mW was applied to the heating resistor and the temperature was measured at the center of the resistor ring. The heating speed was 6.3 K/s (69 GHz/s) for a chip having dimensions of 10 mm × 5 mm × 380 ㎜. The speed increased to 12.7 K/s (140 GHz/s) for a chip having dimensions of 5 mm × 5 mm × 380 ㎜ [93].

# 4 Frequency chirping of optical transmitters

Semiconductor lasers – also known as diode lasers - have many outstanding features over other types of lasers. They are compact, efficient, and cost-effective. In addition, they exhibit attractive tuning and modulation characteristics. Lasing in semiconductors was discovered in 1962 [50,51] and since then the development of these devices for various applications has proceeded rapidly. The use of diode lasers in optical telecommunications took its pace after the development of low-loss optical fiber in the seventies [52] and with the introduction of the erbium-doped fiber amplifier (EDFA) in 1980's by the University of Southampton [53,54]. After the invention of the EDFA, the development of laser transmitters for WDM applications in the 1550 nm band exploded.

The modulation performance of a diode laser is characterized by parameters such as average output power, wavelength and modulation bandwidth. Modulation of the intensity of light causes changes in its optical frequency. These variations are commonly referred to as frequency chirping. The frequency chirp characteristics can provide fundamental knowledge about the operation of the laser under direct current modulation. The chirping characteristics should be accurately modeled and measured for efficient modeling of the laser diode as a transmitter in an optical transmission system. The operation of a diode laser under current modulation can be described with the help of rate equations [55-58]. These equations describe the evolution of a single lasing mode within the laser cavity. The rate equations couple the changes in the concentration of electrons and photons in the active area of the laser. Utilizing the rate equations, the frequency chirp can be related to the output power of the laser diode. This relation can be written as [55,56,63]

$$\Delta n(t) = \frac{a}{4p}\left(\frac{1}{P(t)}\frac{dP(t)}{dt} + kP(t)\right), \qquad (20)$$

where $a$ is the linewidth enhancement factor, $P$ is the output power from the diode laser and $k$ is an adiabatic chirp factor which depends on the laser parameters. The physical implication of the linewidth enhancement factor is that it couples the changes in the real and imaginary parts of the refractive index [59-61]. Frequency chirp can be divided into two components, which are often referred to as adiabatic chirp and transient chirp [62,63]. The adiabatic chirp causes the frequency of the laser to follow the waveform of the output power. Adiabatic chirp induces an offset between the frequencies of the one and the zero states of the laser transmitting on-off modulated signal. Transient chirp occurs during the fast transitions of the output power. In other words, it is dominating during the transition from the zero to the one state and during the transition back from the one state. It has been shown that the transient chirping is more harmful in digital communication systems than adiabatic chirping [62,63]. This is due to the fact, that transient chirping will broaden the pulses whereas the adiabatic chirp tends to shift the pulses in time. Broadening of the pulses leads to degradation of the signal.

The rate equations can be solved only numerically in a case of arbitrarily shaped modulation currents. A number of commercial simulation tools for diode lasers are available. They include models for various kinds of components, which are essential building blocks of modern telecommunication systems. These simulators allow the operation of a complete system to be numerically modeled and its performance to be optimized. During the course of this thesis, the simulator program *Gigabit Optical Link Designer* (GOLD) was used [38]. It can be configured to include a model for frequency chirp according to Eq. (20). When the laser is modulated with a digital signal the modulation depth is characterized by the

extinction ratio. It is the ratio of the average power in the state “1” and the state “0” of the optical signal and is usually given in decibels [21]. Two simulated examples of the output power and frequency chirp of a digitally modulated laser diode are presented in Fig. 8. In Fig. 8a the laser diode is biased with a current of $I_b$=2.0$I_{th}$ and the extinction ratio is set to 8.0 dB. The frequency chirp in this case is primarily adiabatic and it follows the output power of the laser. In Fig. 8b the laser diode is biased with a same current but higher amplitude of the modulation resulting in an extinction ratio of 10.0 dB. It can be observed that when the extinction ratio of the transmitter is increased the transient chirp also increases.

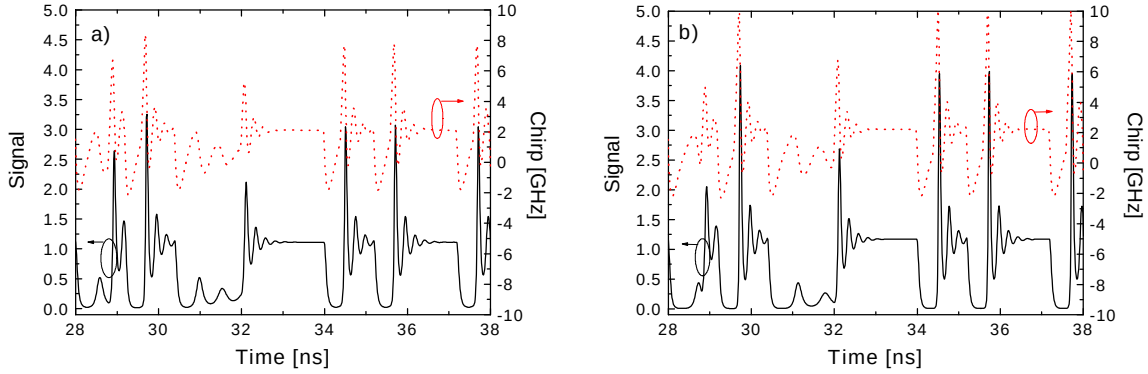


**Figure 8.** Output power and frequency chirp of the directly modulated diode laser with a) an extinction ratio of 8.0 dB and b) an extinction ratio of 10.0 dB.

### 4.1 Measurement methods for the frequency chirp

The frequency of the optical radiation is so high that it cannot be measured directly. The property of light that can be determined is its intensity. Therefore, methods to measure the frequency of the light are often based on transforming the variations in the frequency in fluctuations in the intensity. When an optical intensity modulated pulse containing several frequency components is transmitted through a dispersive medium, the output pulse will be distorted in time. This fact can be used to characterize the amount of frequency chirp of the input pulse [64-68]. However, it cannot be used to resolve the frequency chirping as a function of time. For this purpose several different techniques have been developed.

The conventional method of time-resolved chirp measurement involves detecting the time trace of a repetitive light pulse transmitted through an optical filter with a tunable transmission frequency. By tuning the filter over the whole spectrum of the optical signal a frequency versus time map of the pulse can be generated [69-72]. If it suffices to be able to characterize only the shift of the center-frequency of the pulse, various types of optical frequency discriminators can be applied to convert frequency variations into intensity changes. Several types of interferometers, such as a fiber-optic Mach-Zehnder interferometer [73,74], a Michelson interferometer [75], a birefringent fiber interferometer [76] or a Fabry-Perot interferometer [77,78] have successfully been used for this purpose. In general, the utilization of a frequency discriminator is limited by the dispersion and the time delay inside the component. Also the measurements of very short pulses are limited by the speed of the electronics at the detection side. Therefore, the frequency discriminator can be only applied to signals having a limited repetition frequency and sufficiently long pulse width.

Several techniques have been introduced to characterize the amplitude and frequency characteristics of short pulses. One way is to apply a modulated Mach-Zehnder interferometer as a frequency discriminator. By measuring the optical spectrum from the output of the interferometer at several bias points along its sinusoidal transfer function, the

time-resolved amplitude and phase information can be reconstructed by a recursive algorithm [79,80]. However, this method applies only for periodical pulse trains with a high repetition rate and the optical spectrum must be measured with a high resolution. Another well-established measurement technique is the so-called frequency resolved optical gating (FROG). It resembles an autocorrelation measurement but in addition to the information about the intensity of the pulse, its frequency chirp can be obtained by filtering [81]. Measurement of frequency chirp employing the FROG technique requires the use of sufficiently high optical power, since the operation of the device utilizes second harmonic generation in a nonlinear crystal.

The use of a frequency discriminator offers a straightforward way to measure frequency chirp of various signals without limitations of their periodicity or shape. This permits effects depending on a specific pattern of bits to be explored. The principle of the measurement of frequency variations with an optical filter applied as a frequency discriminator is illustrated in Fig. 9. The signal exhibiting frequency modulation passes through the discriminator, which is biased to either slope of the transfer function. The variation in the frequency induces a change in the transmission of light through the device, which can be observed as a variation in the intensity. When the slope of the discriminator is known the frequency modulation of the signal can be calculated from the measured intensity variation.

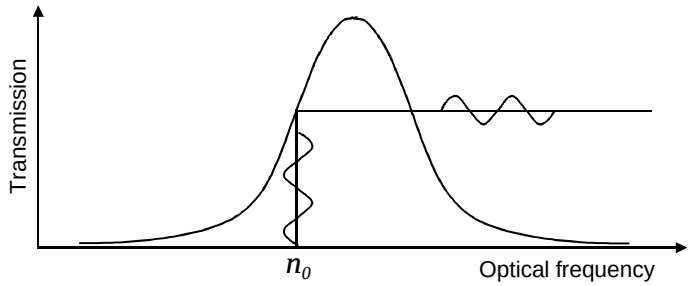


**Figure 9.** Operation principle of an optical filter used as the frequency discriminator.

### 4.2 Silicon wafer etalon as a frequency discriminator

In this thesis, a chirp analyzer is developed utilizing a tunable Fabry-Perot etalon as the frequency discriminator. A temperature-tunable solid etalon made from silicon provides stability against mechanical vibrations and variations in the ambient temperature. We applied two etalons with different thickness of the cavity. The etalon used in the first prototype of the chirp analyzer was fabricated from a silicon wafer with a thickness of ~500 *m*m [P3]. The thickness of second etalon was ~650 *m*m [P4]. The reflective mirrors are provided simply by the polished silicon surface without coating. The etalon was inserted in the air-gap of a fiber-optic beam expander. The transmission spectrum of the etalon was measured with spontaneous emission noise from an EDFA and an optical spectrum analyzer. The transmission spectrum of the second etalon is shown in Fig. 10. The transmission follows the Airy function, which was fitted to the measured data for estimating the reflectivity *R* and the *FSR* of the etalon. The reflectivity of the mirrors of *R*=0.28 and *FSR*=62 GHz were obtained from this fit.

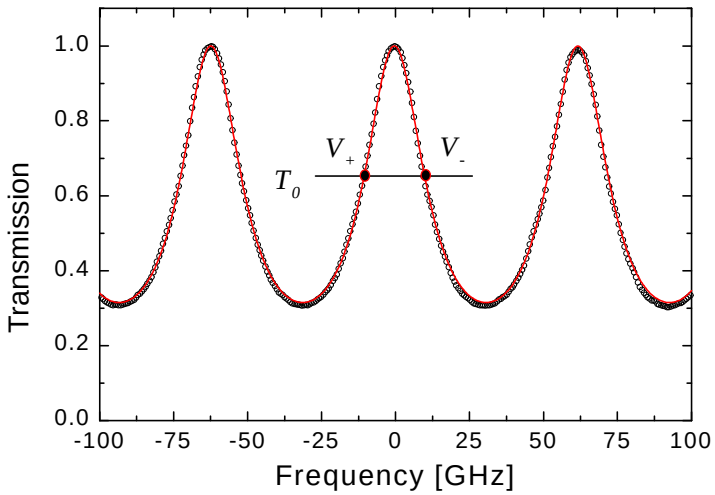


**Figure 10.** Transmission spectrum of the Fabry-Perot etalon utilized as the frequency discriminator. The operation points $V_+$ and $V_-$ are selected for determination of the frequency chirp. [P4]

The frequency chirp on the intensity-modulated signal can be calculated from the data measured at both the positive $V_+$ and the negative slope $V_-$ of the transmission fringe. The operation point is selected from the middle of the fringe according to the relation $T_0=(T_{MAX}+T_{MIN})/2$. The frequency chirp can then be calculated from [78]

$$\frac{V_+(t)-V_-(t)}{V_+(t)+V_-(t)}=\frac{(1-R)\sqrt{(1-T_0)\cdot(T_0(1+R)^2-(1-R)^2)}\sin(2p\Delta n(t)/FSR)}{T_0(1+R^2)-(T_0(1+R^2)-(1-R)^2)\cdot\cos(2p\Delta n(t)/FSR)}, \qquad (21)$$

where $FSR$ is the free spectral range of the etalon and $R$ is the reflectivity of the mirrors and $T_0$ is the selected operation point of the etalon. This equation can be simplified if the frequency chirp is small i.e. $\Delta n<<FSR/2$. The equation for the chirp can then be written as

$$\Delta n(t)\approx\frac{FSR}{2p}\frac{V_+(t)-V_-(t)}{V_+(t)+V_-(t)}\left[(1-T_0)\left[T_0\frac{(1+R)^2}{(1-R)^2}-1\right]\right]^{-1/2}. \qquad (22)$$

The frequency resolution and the temporal resolution of the etalon can be selected to optimize the performance of the discriminator for the desired application. The trade-off between the wavelength and time resolution can be expressed as a time-bandwidth product. For Fabry-Perot etalons this product is approximately independent of the reflectivity and the length of the cavity. It can be written as [71]

$$\Delta t\Delta n=\frac{\ln\sqrt{2}}{p}=0.11, \qquad (23)$$

where $\Delta\tau$ and $\Delta\nu$ are *FWHM* widths of the impulse response and the transmission fringe of the etalon. This expression sets the transform limit of the Fabry-Perot etalons.

### 4.3 Real-time measurement of frequency chirp

Applying only one etalon does not allow for measuring frequency chirp of the optical transmitter in real time. This due to the fact that if the parameters of the laser vary the measurement device needs to be re-initialized. Moreover, since the measurements have to be performed at both the negative and positive slopes of the filter transmission curve two discriminators are required to perform the measurement. Real-time measurements have been

conducted with a waveguide grating router (WGR), also known as an arrayed waveguide grating (AWG) [82]. This filter separates the input light into separate channels. The shape of the passband of the device is nearly Gaussian. When the wavelength of the signal is tuned between adjacent channels the device provides frequency discrimination on both the positive and negative slope simultaneously. When the signals from the two channels are measured, it is possible to extract the frequency modulation of the original signal. However, this method operates for a fixed wavelength at a time and tuning to another is relatively slow. To improve the method of measuring the frequency chirp, we have developed a real-time method to measure the frequency chirp of the transmitters. The method is based on using two similar etalons. Their transmission is tuned in such a way that one of the etalons has its transmission at the positive slope and the other has its transmission at the negative slope. The measurement setup to realize such a configuration is displayed in Fig. 11. The advantages of this system include real-time operation and the analyzer can measure frequency chirp even if the operation conditions of the laser are changed. These variations can be the variation of the wavelength, extinction ratio or average power of the signal. The system needs to be calibrated for the difference in the length of the arms of the measurement system and for the differences in the attenuation of the signals. The frequency response of the detectors should be sufficiently similar.

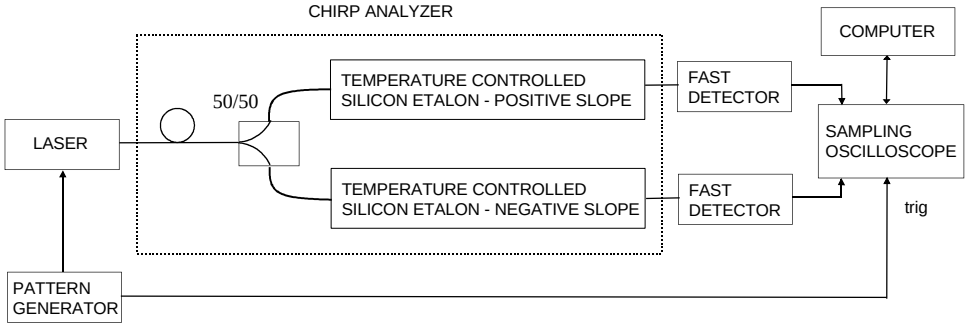


**Figure 11.** Setup for realization of real-time frequency chirp measurements utilizing two temperature-controlled silicon etalons [P4].

### 4.4 Examples of frequency chirp of directly modulated lasers

The chirp analyzer proved to be a useful tool in characterization of the chirping of directly modulated lasers. Measurements were primarily conducted for digitally modulated transmitters applied for synchronous digital hierarchy (SDH) applications and common antenna television (CATV) transmitters, which are modulated with an analog signal. The frequency-chirping characteristic of directly modulated lasers can be estimated from the output power by Eq. (20) [83]. It can be deduced that when the laser is biased well above the threshold current and the modulation index (extinction ratio) is small then the transient chirp will be small and the laser exhibits mainly adiabatic chirp. However, if the bias is reduced or the modulation index is increased then transient chirp will be present and its effect will dominate during fast changes of the signal waveform. An example of frequency chirp in digitally modulated laser diodes is given in Fig. 12. The bit-rate is 2.5 Gbit/s. The measurement was performed for two different extinction ratios. The effect of reducing the bias can be observed as an increase of the transient chirp during the fast transitions of the signal.

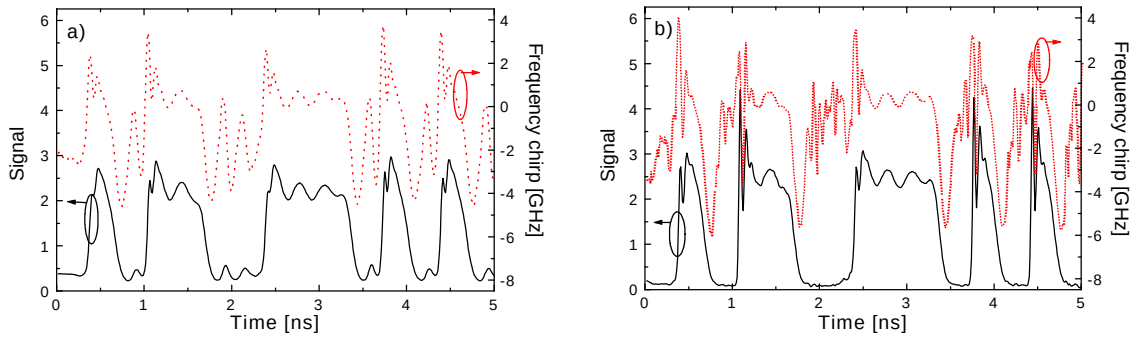


**Figure 12.** a) Frequency chirp of a laser modulated with a digital signal (Lucent, output power +1 dBm, extinction ratio 7 dB). b) Frequency chirp of a laser modulated with an analog signal (Lucent, output power +1 dBm, extinction ratio 13 dB).

Measured waveforms and the corresponding frequency chirp of a CATV laser with analog modulation is presented in Fig. 13. For sinusoidal signal the depth of modulation is often expressed by the optical modulation index (OMI) defined as OMI=($P_{max}$-$P_{min}$)/(2$P_{ave}$), where $P_{max}$-$P_{min}$ is the peak-to-peak value of the signal power and $P_{ave}$ is the average power. Also for sinusoidal modulation the change in the operation conditions of the laser has a significant influence on the transient chirp. It can be pointed out that the transient chirp begins to display severe relaxation oscillation even when no significant changes in the signal waveform can be observed. This can be explained by the fact that frequency modulation increases near the relaxation oscillation frequency more rapidly than intensity modulation [56].

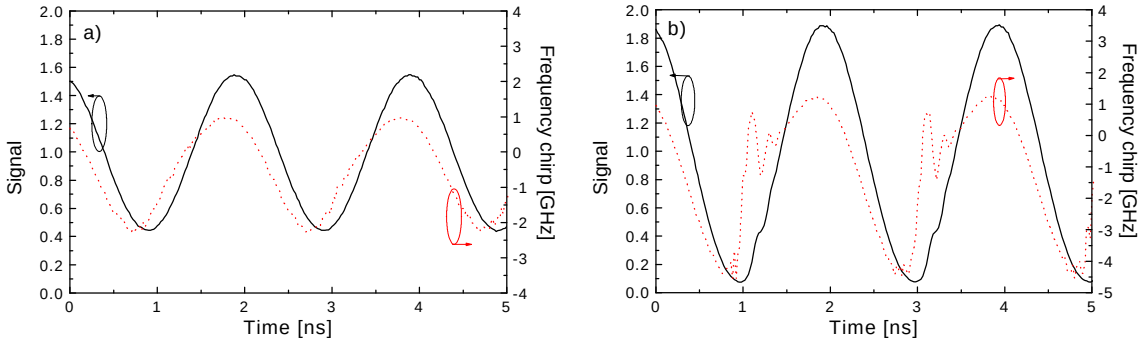


**Figure 13.** a) Frequency chirp of a laser modulated with an analog signal (Sumitomo, $P_{ave}$=+5dBm, 500 MHz, OMI 56%). b) Frequency chirp of a laser modulated with an analog signal (Sumitomo, $P_{ave}$ =+5dBm, 500 MHz, OMI 90%) [84].

The effects of frequency chirp in the system are mainly related to the dispersion-induced pulse broadening in the anomalous dispersion region of the standard single-mode fiber [85,86]. The amount of frequency chirp in a laser can be affected by making a suitable selection of the value for the extinction ratio. Extensive work carried out through simulations and experiments have lead to the proposal that the extinction ratio should be within 7.8 dB – 9.4 dB for directly modulated transmitters [87]. Tolerance of the receiver against the dispersion induced broadening of the signal pulses can be partly enhanced by increasing the average power of the signal. The dispersion-induced penalty is defined as an increase in the optical power at the receiver in order to achieve the same level of performance as without the dispersive fiber. The dispersion penalty is increased and in a worst case, a bit-error-rate floor is generated due to pattern dependent effects and chirp noise [88,89].

In analog systems where diode lasers are employed as optical transmitters, the requirements for the signal quality are extremely strict. In case of directly modulated lasers as the transmitters, the transmission range is limited to about only 6 km due to dispersion of the standard single-mode fiber [90,91]. However, directly modulated lasers can efficiently be applied in distribution of digital television channels, which use quadrature amplitude modulation [84].

# 5 Spectral filtering

The transmission properties of directly modulated diode lasers can be improved if the broadening of the optical spectrum induced by frequency chirp is suppressed. Filtering has successfully been applied to extend the transmission distance in dispersive fibers and reduce intersymbol interference. Different types of filters, such as Fabry-Perot interferometers have been demonstrated to operate for such a purpose [92,93]. Also, fiber Bragg gratings and filters based on the diffraction gratings have shown to be suitable [94-98]. Spectral filtering has also been studied as a way to improve the properties of other semiconductor devices. One example of such a device is a wavelength converter based on a semiconductor optical amplifier. Filtering of the spectrum of the converted signal results in that the quality of the intensity modulated signal is improved and the penalties are decreased.

## 5.1 Spectral filtering of directly modulated diode lasers

In the course of this thesis, an optical filter similar to the one applied in the measurement of frequency chirp was further developed. This new filter has dielectric mirrors deposited on the surfaces of the silicon wafer to increase the reflectivity. The thin-films for the mirrors were formed with plasma-enhanced chemical vapor deposition (PECVD). This technique is well suited for thin-film deposition of materials such as SiN, $SiO_2$ and SiON. The mirrors were fabricated from a stack of three layer pair of $SiO_2$ and $Si_3N_4$ having a thickness of a quarter of a wavelength.

The construction and the physical dimensions of the filter are displayed in Fig. 14a. The reflectivity of the mirrors and the *FSR* was determined by fitting an Airy function to the measured transmission spectrum of the filter. The reflection obtained from the fit is $R$=0.66 and the *FSR* is 110 GHz at the wavelength of 1550 nm [P6] (see Fig. 14b). The measured *FSR* indicates the thickness of the cavity to be ~380 *m*m.

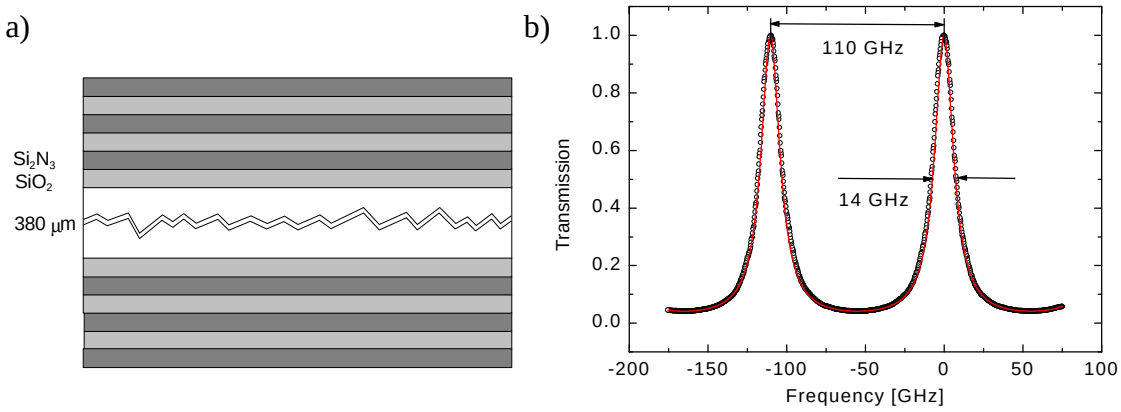


**Figure 14.** a) Construction of the temperature-tunable Fabry-Perot etalon. b) Measured transmission spectrum (*open circles*) and the fitted Airy-function (*solid line*).

The experimental setup for testing the operation of the filtering in a point-to-point link is shown in Fig. 15a. The laser transmitter was modulated with a bit-rate of 2.5 Gbit/s using pseudo-random-binary sequence having a word length of $2^{31}$-1. The filter was placed after the transmitter and its operation point was tuned to several values. The total length of the fiber link was 350 km and three EDFAs were used to amplify the signal. The bit-error-rate

(BER) was measured after the link for different receiver powers. The measured BER curves are shown in Fig. 15b. The reference receiver sensitivity without the amplifiers and the fiber is given by back-to-back measurement (B-to-B). Dispersion penalty is the increase in the power required to achieve an adequate BER of $10^{-9}$. When filtering was applied, the receiver sensitivity could be improved by 1.5 dB when the operation point was set at the slope of the filter [P6].

a)

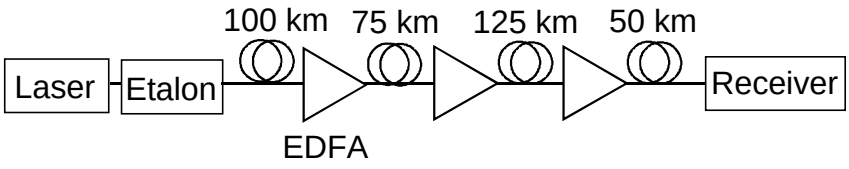


b)

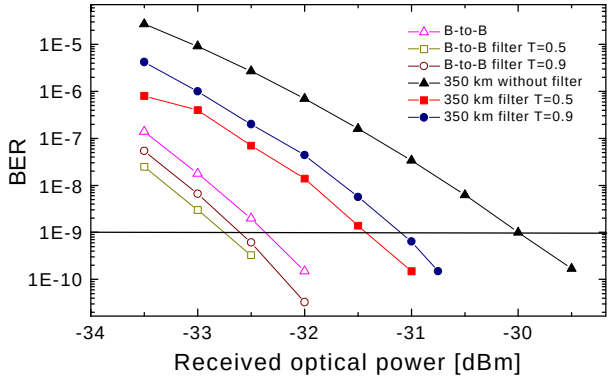


**Figure 15.** a) Experimental setup for testing spectral filtering. b) Results of BER measurements for different operation points of the filter.

When the signal having adiabatic frequency chirp passes through the slope of the filter the extinction ratio of the signal will be increased. The increased extinction ratio indicates directly an improvement in the BER performance. On the other hand, the extinction ratio can be tuned to a smaller value already at the transmitter, which causes less chirping. After the filter, the extinction ratio will be improved to an acceptable level. In the case of adiabatic chirp, the optimum operation-point along the filter transmission is where the slope is steepest. In the case of transient chirping the optimum operation-point is at the peak of the transmission curve of the filter. In our experiments, we used a relatively low speed of modulation. With this speed we did not observe significant changes in the frequency chirp of the signal after the spectral filtering. This was observed by both simulations and experimental measurements [93].

### 5.2 Gain-switching of laser diodes

Short optical pulses have several applications in the field of optical measurements and optical communications. Short pulses can be generated, for example, by using mode-locked laser diodes, mode-locked fiber lasers and gain-switched laser diodes. Mode locking of fiber lasers can be accomplished with either active or passive mode-locking techniques. By using passive mode-locking schemes, very short pulse widths of 100 fs can be readily achieved [99,100]. However, the repetition rate of the passively mode locked laser are often not very high which limits their usability in optical telecommunication applications. To overcome this limitation, actively mode-locked fiber lasers are applied. The repetition rate of an actively mode-locked fiber laser can be very high, typically repetition rates of 10-40 GHz can be achieved [101,102].

The use of fiber lasers for generating short pulses is an efficient way but it is also expensive and very sensitive to environmental fluctuations. Another way of generating short pulses is gain-switching of the diode lasers. This method can be applied to generate stable pulse-trains with a simple configuration [103-108]. The widths of the pulses can be on the order of a few picoseconds. Basically, gain switching is simply another form of direct modulation of the diode lasers. Possibility to generate pulses, which are shorter than the elecrical pulses driving the diode laser was realized when the relaxation oscillation of the lasers was observed. The basic idea of gain switching is to excite the first relaxation oscillation peak and then cut of the electrical current before the second oscillation peak appears. When the gain is suppressed below the lasing threshold by cutting out the injection current the relaxation peaks following the first one are eliminated resulting in a generation of a single short pulse. The mechanism for the generation of gain switched pulses is illustrated in Fig. 16a. In this example the laser diode is biased below the threshold current and modulated with a sinusoidal current having a high amplitude [104,105]. The sinusoidal current $I_{MOD}$ starts to generate carriers $N$ inside the active region of the cavity. When the number of carriers increases above the threshold $N_{\mathrm{th}}$ for laser operation the photon population starts to increase rapidly and optical power is generated in a form of the first peak of the relaxation oscillation. The generation of photons consumes the electron population fast and this effect is enhanced since the sinusoidal current modulation starts to decrease and the number of carriers gets fast below the threshold of the laser operation. This way the second and all of the subsequent relaxation oscillation peaks are suppressed and the output power from the laser consists of narrow pulses with repetition rate equal to the frequency of the sinusoidal modulation of the injection current. If the bias current is increased, the top of the sinusoidal current will be at such a high level that the second relaxation oscillation period begins to be visible. This situation is illustrated in Fig. 16b.

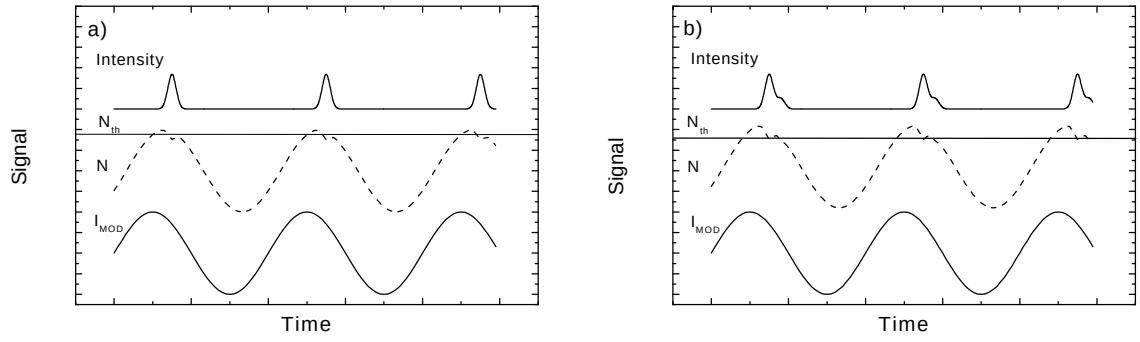


**Figure 16.** a) Principle of operation of pulse generation by using gain-switching of a diode laser. b) Pulse formation with higher bias current.

The electrical pulse waveform does not need to be sinusoidal but almost any pulse waveform can be used [107,108]. The setup for generation and analysis of the gain switched pulses is displayed in Fig. 17. The optical spectrum of the pulses can be measured with an optical spectrum analyzer and the shape of the pulses can be investigated with a fast photodetector and a digital sampling oscilloscope. The temporal resolution of the measurement setup is limited by the bandwidth of the detector and the oscilloscope. The resolution of the measurement device can be approximated with a rise-time of the signal. The rise-time $t_{\mathrm{r}}$ of a device having a bandwidth of $B$ (GHz) can be approximated from the relation, $t_{\mathrm{r}}$=350 ps/$B$. Therefore the measurement of the pulsewidth of the system system having a electrical bandwidth of $B$=40 GHz is limited to 17.5 ps. If pulses are shorter, their width can not be

measured by electrical means. A more accurate method with a much higher resolution is an autocorrelator, which can be used to measure pulsewidth down to a few femtoseconds.

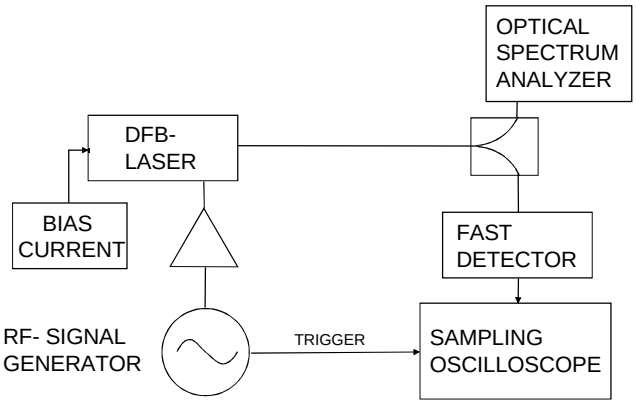


**Figure 17.** Setup for generation and characterization of gain-switched pulses.

One of the most important applications of short pulses is the generation of optical solitons for long-haul communication systems. Solitons are pulses, which propagate in an anomalous dispersion region of optical fiber without changing their shape. This is possible due to the interplay between the dispersion and optical nonlinearities [109]. The formation of solitons inside the optical fiber requires that the launched pulses are nearly transform limited. The transform limit indicates that the spectrum of the pulses is directly given by the Fourier transform of its intensity. However, the gain-switched pulses have a large frequency chirp which is characteristic to direct modulation of the laser diode. As a consequence of the chirping the optical spectrum broadens above the transform limit. If the shape of the output pulse is Gaussian and the chirp is mainly transient chirp, it can be shown from the Eq. (20) that the pulses exhibit linear negative chirp. The frequency is higher at the leading edge of the pulse than at the trailing edge. This type of linear frequency chirp can be compensated by launching the pulses into the optical fiber having normal dispersion [109,110]. Normal dispersion induces frequency chirp which is opposite in sign to that of the initial pulse leading the pulse properties close to the transform limit.

### 5.3 Spectral filtering of gain-switched pulses

Spectral filtering can be applied also to modify the spectral properties of the pulses produced by gain switching of diode lasers. Gain switching produces short pulses, which have large frequency chirp. In order to apply these pulses in optical communication systems or in optical measurements, it is desirable that the pulses are transform limited. Transform limit indicates that the spectrum of the signal is directly obtained from the Fourier transform of the signal waveform. In other words, this means that the signal does not have frequency chirp. To produce transform-limited pulses from gain-switched lasers, the signal spectrum can be filtered to suppress the frequency variation. There exist mainly two methods to obtain transform-limited pulses from the chirped gain-switched pulses. One way is to use a narrowband optical filter to suppress the spectrum of the signal [111-113]. Another approach is to employ an optical fiber with normal dispersion to induce linear chirp, which is opposite to that of the original pulse [109,114-116]. Besides these basic methods some advanced pulse compression methods can be used to compress the width of the pulses [117].

The basic effects of optical filtering on the chirping characteristics of the gain-switched pulses can be modeled by considering simplified Gaussian pulse shape and linear frequency chirp. An example of filtering can be illustrated by making a numerical model using Gaussian pulses [P5]. The full-width-at-half-maximum (FWHM) width of the pulses in this example was set to $t_0$=39 ps. The pulses were transmitted through an optical Fabry-Perot

etalon filter, which was modeled in the time domain by its impulse response. The output field can be presented as [P5]

$$E_{OUT}(t) = E_0(1-R)\sum_{n=0}^{\infty} R^n \cdot e^{-j\frac{w_0}{FSR}n} \cdot e^{-\frac{1}{2T_0{}^2}(t-\frac{n}{FSR})^2} \cdot e^{jpC(t-\frac{n}{FSR})^2}, \qquad (24)$$

where $w_0$ is the center angular frequency of the filter $T_0$ is 1/e-width of the Gaussian pulse and $C$ is the linear chirp rate. The reflectivity $R$ is 0.66 and the $FSR$ is 110 GHz corresponding the values of our etalon. The results for the linearly chirped pulse having a chirp rate of $C$=-750 MHz/ps transversing the etalon at three different settings of the center frequency of the etalon filter are shown in Fig. 18. The center frequency of the passband of the filter was set to values the 0 GHz, -30 GHz and 30 GHz. This clearly illustrates the effects of the center frequency of the filter on the temporal shape of the pulses. The original pulse with a perfectly linear frequency chirp is displayed in Fig. 18a. The chirp in the filtered signal is changing due to the optical filtering as can be observed in Figs. 18b, 18c and 18d. When the center wavelength of the filter was tuned to –30 GHz position, where the pulse is broadened to its maximum value, the chirp remains first almost unchanged until its value starts to decrease towards the trailing edge of the pulse. When the filter is tuned to the center position (0 GHz) the chirp within the duration of the pulse is reduced. When the filter was tuned to produce a compressed pulse (30 GHz) that has secondary peaks, the frequency chirp exhibits very large peaks that are located at the minimum points between the secondary peaks in the pulse profile.

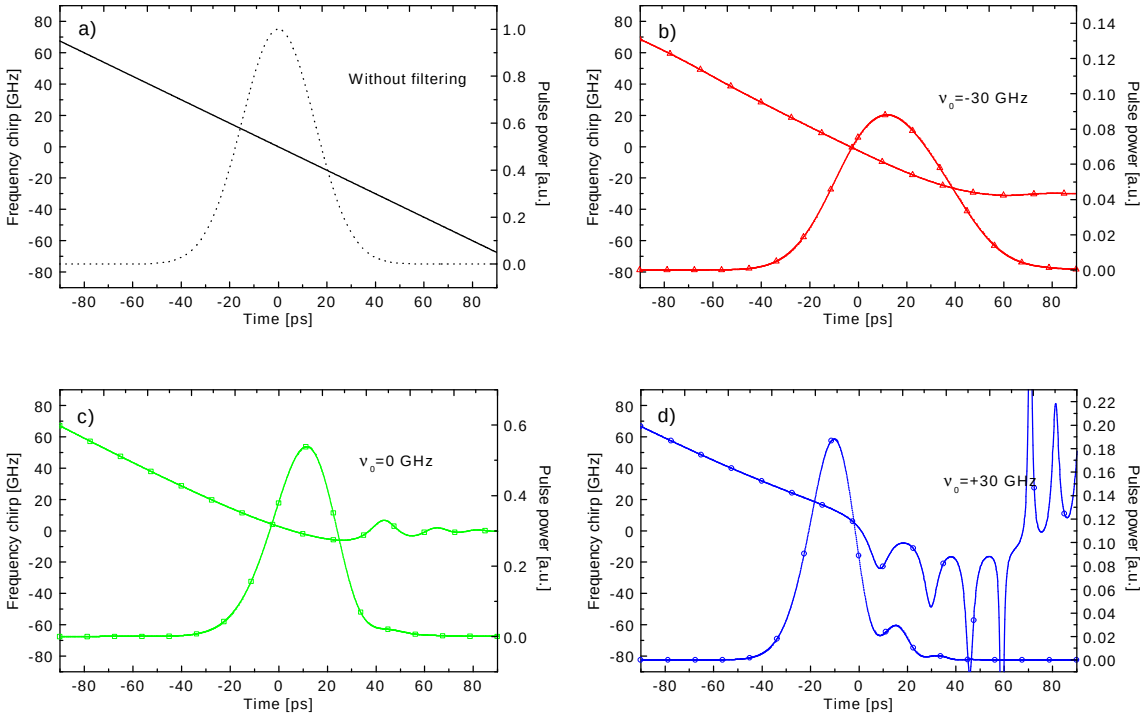


**Figure 18.** Pulse waveforms (*dotted lines*) and the corresponding frequency chirps (*solid lines*) of the filtered signal.

The broadening and compression of the pulses displayed in Figs. 18b and 18d can also partly be explained by the dispersion of the etalon cavity. Since the chirp during the pulse is negative, the pulse will be broadened due to anomalous dispersion. When the center frequency of the filter was tuned to a position of –30 GHz, the spectrum of the pulse will experience normal dispersion and its width will broaden (Fig. 18b). Whereas a tuning in the

opposite direction will lead to a compression of the width of the pulse as can be observed from Fig. 18d. These changes in the shape of the pulses were experimentally observed by filtering the pulses generated with a DFB-laser diode [P5].

# 6 Wavelength monitoring

Measurement and control of the wavelength of optical transmitters are important issues for maintaining the reliability of optical networks. Optical monitoring of the wavelength can be accomplished with wavemeters or optical spectrum analyzers. However, these devices are expensive and bulky for active use of monitoring the transmitter wavelengths. Currently employed ways to implement a low-cost system include both fixed and tunable filters [118-120]. In the course of this thesis, schemes to actively monitor the wavelengths of a single transmitter or a number of WDM channels simultaneously were investigated utilizing the temperature-tunable Fabry-Perot filter described in the previous sections.

## 6.1 Monitoring of a single wavelength

The temperature-sensing resistor integrated on the surface of the filter allows a convenient means to monitor changes in its temperature. The laser wavelength was locked to the slope of the filter by keeping the transmission of the laser light at a constant operation point. Changes in the temperature of the filter chip can then be directly related to the changes in the wavelength of the transmitter. The experimental setup for locking the transmission of the filter is depicted in Fig. 19a. In this scheme, the light from the source passes through the filter and a small portion of the signal power was coupled out before and after it. By providing a feedback loop to maintain the ratio of these powers constant, the changes in the wavelength of the transmitter can be monitored in real time. The changes in the wavelength of the transmitter can be deduced from the changes of the resistance of the temperature-sensing resistor. For accurate characterization, the sensor resistance versus wavelength curve needs to be calibrated. The calibration was performed by feeding light from a wavelength tunable laser through the filter and by measuring the accurate wavelength of the laser with a wavemeter. The measured change of the sensor resistance as a function of the wavelength of a tunable laser while the operation point was locked to the slope of the transmission is displayed in Fig. 19b. The sensitivity of the resistance to the wavelength change was obtained by fitting a line to the measured data. The relation was found to be linear with a sensitivity of 37 ohm/nm and the standard deviation of the fit was ~2 pm. This monitoring scheme should be very convenient to use for single-channel transmitters if the etalon is inserted inside the package of the laser transmitter.

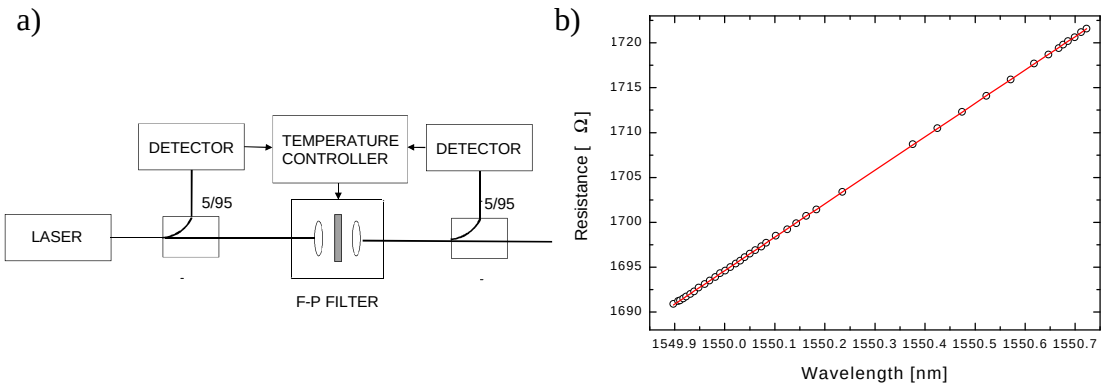


**Figure 19.** a) Setup for monitoring the wavelength of a single laser transmitter. b) Sensitivity of the resistance as a function of the wavelength drift.

### 6.2 Monitoring of multiple wavelengths

Monitoring of multiple channels has been demonstrated by applying a Fabry-Perot etalon and pilot tones to identify each of the channels in the WDM-network [121,122]. The slope between the channels in an AWG has also been used to monitor the changes in the wavelengths of multiple signals [123]. Recently, we proposed a scheme for monitoring the wavelengths of a WDM-system using one single Fabry-Perot etalon [124].

The transmission spectrum of the Fabry-Perot etalon was first stabilized by locking one of its transmission fringes to a laser stabilized to an absorption line of acetylene to provide an accurate wavelength reference. The DWDM-wavelengths were sent through the filter and a small portion of power was tapped off before and after it. The output light from the acetylene-stabilized reference laser was transmitted within one of the channels in an 8-channel DWDM-system. The tapped off wavelengths were divided by using multiplexers (MUXs) and the stabilized laser locked the etalon filter by tuning its temperature to maintain the transmission constant within the reference channel. The setup for filter locking and wavelength monitoring is given in Fig. 20a. The wavelength shifts were traced by detecting changes in the transmission of the laser within the channel to be monitored. The monitoring was realized with a data acquisition card (DAQ) connected to a computer. When the wavelength of the laser in the monitored channel shifts, the changes in its transmission can be directly used to estimate the shift simply by comparing it to the calculated transmission spectrum of the filter. The spectrum of the filter while it was locked to the acetylene-stabilized laser at a wavelength of 1546.174 nm was measured using a broadband source and an optical spectrum analyzer. The measured transmission spectrum of the etalon and two of the WDM-channels are displayed in Fig. 20b. The wavelength of the laser within the monitored channel was swept and its transmission along the sweep is displayed in Fig. 20b with dots. The *FSR* of our etalon is 110 GHz so it does not exactly correspond to the 200 GHz spacing of the WDM channels. Nevertheless, the concept was successfully demonstrated and wavelength shifts of about 1 pm could be detected.

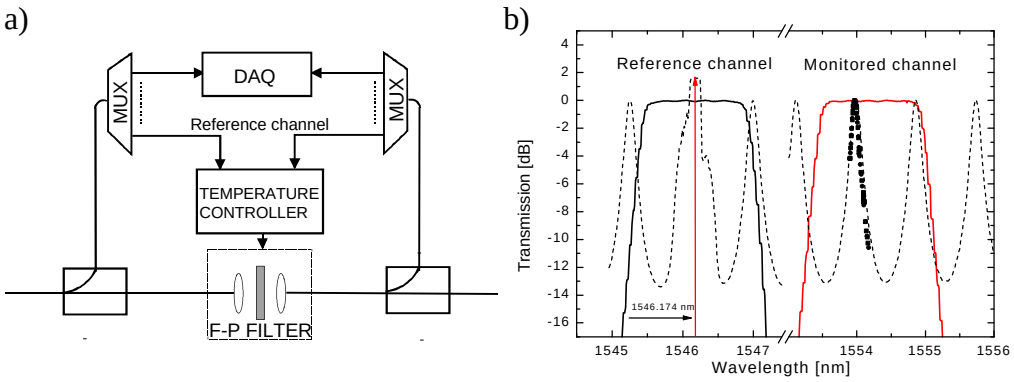


**Figure 20.** a) Setup for wavelength monitoring of a multi-channel DWDM-system. b) Two DWDM-channels (*solid line*), the measured filter transmission (*dashed line*) and the measured change in transmission at the monitored channel (*dots*).

# 7 Wavelength reference

Accurate knowledge of the wavelength of an optical source is important in calibration of measurement devices such as optical spectrum analyzers and wavemeters. Calibration services of these devices are offered nationally by certified calibration laboratories which maintain the reference for the optical wavelength scale. A need for a reference artifact for wavelength calibrations and monitoring has been recognized by ITU [125]. Their recommendation summarizes some of the possible applications of the reference artifact as:

1) Calibration of WDM test equipment
2) Providing a frequency reference for fabrication and calibration of WDM devices
3) Directly providing a reference frequency to multichannel systems
4) Controlling and/or maintaining optical-source frequencies.

During recent years, several devices and materials to realize an accurate wavelength reference have been proposed. However, no detailed proposal on how to realize such an artifact has been yet given by any standardization organizations. Currently, there are two ongoing projects with the objective to develop a reference artifact for practical calibration and wavelength monitoring applications over a wide wavelength range. One of these entitled *Certified Reference Materials* is funded by the European Union [126] and the other entitled *Optical Communication Wavelength References* by the Nordic Industrial Fund, in which the Fiber-Optics Group of HUT is one of the three participants. Presently, a relative accuracy of $10^{-6}$ of the reference is sufficient for calibration of most wavemeters and optical spectrum analyzers. The accuracy needed in laboratory references for metrological applications is of the order of $10^{-12}$. In this thesis, we propose and demonstrate a simple wavelength reference artifact with an adequate accuracy for calibration and monitoring of field instruments.

## 7.1 Interferometers as relative wavelength references

Stable optical resonators such as Fabry-Perot interferometers are widely used as relative wavelength and frequency references. A Fabry-Perot interferometer has a large number of identical equidistant resonance peaks. An interferometer can be designed to provide desired properties as a function of wavelength if it is carefully constructed and stabilized against environmental variations. Devices utilized as wavelength references for WDM systems include Michelson interferometers [127] and Fabry-Perot interferometers [128-132]. Recently, also fiber Bragg gratings (FBGs) have successfully been employed. A FBG has one or several reflection bandwidths, which can be applied for referencing purposes when the grating is temperature stabilized. Wavelength reference artifacts based on the use of several FBGs have recently become commercially available [133].

## 7.2 Absorption lines as absolute wavelength references

Molecular and atomic absorption lines offer the prospect of portable absolute frequency references. The uncertainties in the wavelengths of these lines are as low as $10^{-7}$ to $10^{-8}$ for Doppler-broadened lines and even smaller for Doppler-free lines. For telecommunication wavelengths, acetylene, cyanide, methane, carbon monoxide, iodine and water have suitable molecular reference lines [134,135]. The linewidth of Doppler-broadened absorption lines is typically on the order of 2 GHz. It is limited by various broadening mechanisms [136,137]. The accuracy of the wavelength stabilization can be increased by using low gas pressure and stable temperature. Variations in the gas pressure induce both broadening and shift of the absorption line. By locking the laser frequency to a Doppler-broadened absorption line an

accuracy of ~10 MHz at a wavelength range of 1550 nm and a long-term frequency stability of better than $10^{-8}$ can be achieved [138].

The accuracy and stability can be improved by typically two orders of magnitude by applying saturated absorption techniques [139,140]. The most accurate references for optical telecommunication applications have been realized by locking the wavelength of a narrow linewidth laser to a two-photon absorption of rubidium at a wavelength of 778 nm [138,141]. The accuracy with this technique is ~10 kHz and the relative frequency stability is ~$10^{-12}$. However, this approach is presently only suitable for the realization of an absolute reference for laboratory use.

Acetylene and cyanide are suitable reference gases in the 1550 nm region, whereas methane can be utilized in 1310 nm region. The wavelength range in which the absorption lines are strong covers 1515 nm to 1540 nm for acetylene $^{12}C_2H_2$ and approximately 1520 nm to 1555 mn for $^{13}C_2H_2$. The transmission spectrum of an absorption cell with $^{13}C_2H_2$ is shown in Fig. 21. It was measured by scanning the wavelength of a tunable laser over the spectrum and by recording the intensity passing through the absorption cell. The double branch shape of the two regions is characteristic to the absorption spectrum of several gases. These branches are called R and P branch. Accurate wavelengths of the absorption lines have been obtained through spectroscopic measurements [138].

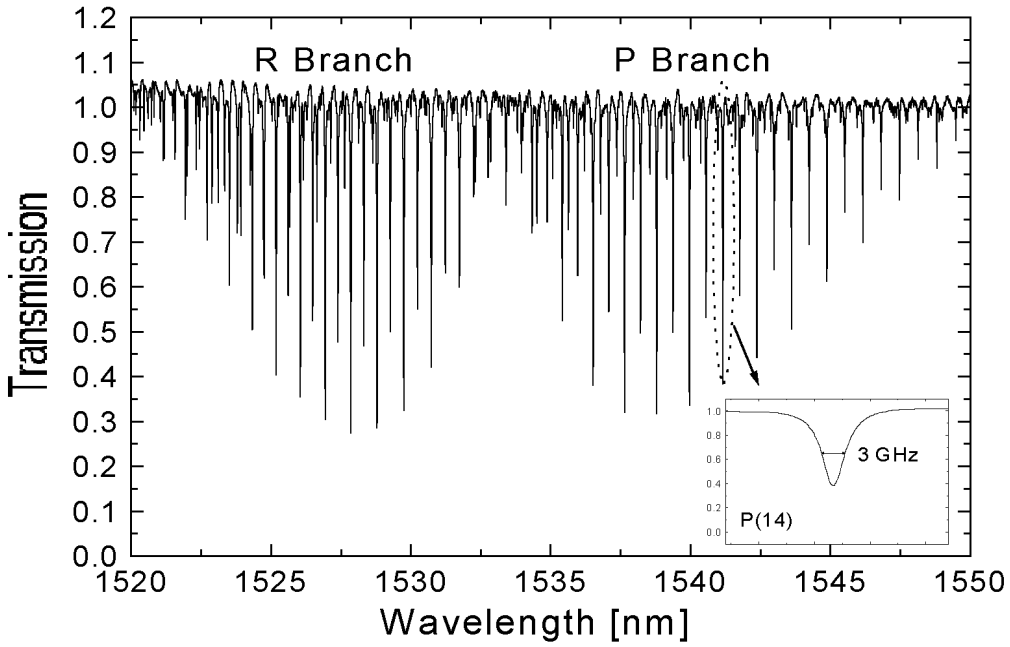


**Figure 21.** Transmission spectrum of an absorption cell with $^{13}C_2H_2$. Lineshape of P(14) line at a wavelength of 1541.167 nm is shown in the insert.

### 7.3 Fabry-Perot silicon etalon as a wavelength reference

The accuracy offered by molecular or atomic absorption lines is high. However, they do not cover a wide wavelength range and they do not exactly match any of the center wavelengths of the WDM channels. On the other hand, the transmission properties of a Fabry-Perot etalon can be tailored to provide a desired set of transmission fringes at accurate wavelengths. Once the properties of the etalon, such as the *FSR* and its wavelength dependence are known, the position of any of the fringes can be calculated. Each of these can then be utilized as an accurate reference point for wavelength calibration or measurement. Since the Fabry-Perot etalon is not an absolute reference, an accurate reference wavelength is

often needed to lock its transmission spectrum. To avoid the use of an absolute reference wavelength, we have investigated the feasibility of using our temperature-tunable Fabry-Perot etalon as a wavelength reference.

Several factors affect the accuracy of a reference based on a solid state material. One of the most important features is the wavelength dependence of the refractive index. This data for silicon can be found from the literature (see Fig. 5b). The Fabry-Perot etalon can be temperature stabilized to provide a set of transmission fringes. The position of these can be calculated with high accuracy for referencing purposes. A change in the *FSR* of the etalon with temperature can be calculated from the relation

$$\frac{dFSR}{dT} = -FSR_0\left(\frac{1}{h}\frac{dh}{dT} + b\right), \tag{25}$$

where $dh/dT$ is the temperature coefficient of the refractive index and $b$ the thermal expansion coefficient of silicon. $FSR_0$ is the free spectral range at a reference wavelength. The effects of the wavelength on *FSR* are shown in Fig. 22 for a value of 110 GHz for $FSR_0$.

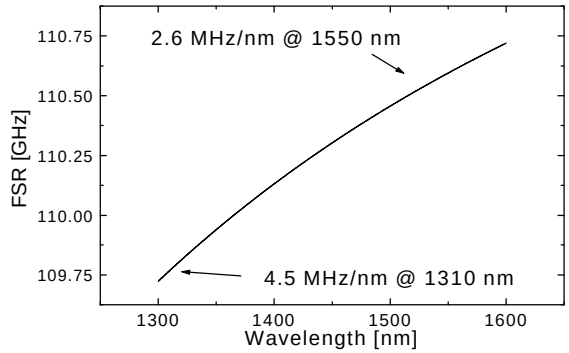


**Figure 22.** Wavelength dependence of the *FSR* due to material dispersion.

The mirrors of the etalon were constructed from dielectric layers, which results in a variation of the *FSR* of the etalon with wavelength. The wavelength-dependent penetration-depth of light to the mirror structure depends on the number of layers and the refractive indices of the mirror materials. The dielectric mirrors may also limit the usable wavelength range of the reference since their reflectivity varies as a function of the wavelength. An analytical calculation of the reflectivity of multi-layer structures at an arbitrary wavelength is not an easy task. Therefore, numerical techniques typically based on a transmission matrix method are often applied to determine the transmission and reflection properties of the thin-film mirror structures [34]. The basic structure of thin-film mirrors deposited on a silicon substrate can be expressed as (S [L H]$^N$ Air), where S denotes silicon substrate, L denotes the low-index material ($SiO_2$, $h$=1.47) and H is the high-index material (SiN $h$=2.1). The number of low and high index layer-pairs is N. The calculated reflectivity of a quarter-wavelength mirror having from 2 to 5 layer-pairs is shown in Fig. 23a. The center wavelength for the mirror reflectivity is set to 1550 nm. The figure illustrates a trade-off between the reflectivity and bandwidth of the mirrors. To be able to use highly reflective 5-layer mirrors in a etalon based wavelength reference over the wavelength range from 1310 nm to 1625 nm the center wavelength needs to be shifted from 1550 nm to lower values. The effect of changes in the reflectivity of the mirrors on the transmission spectrum is displayed in Fig. 23b. In this example the center wavelength for the mirror reflectivity is set to 1390 nm.

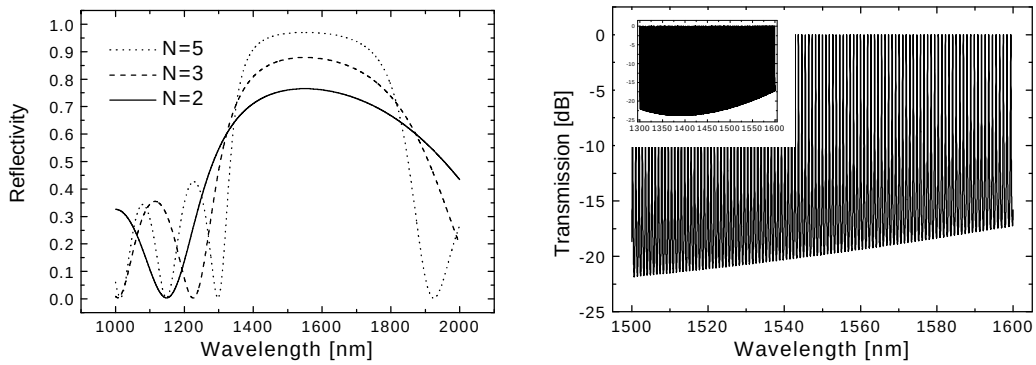


**Figure 23.** a) Reflectivity of quarter-wavelength mirrors for several numbers of layers. b) Transmission spectrum of the etalon having mirrors with N=3 layer pairs. The insert shows the transmission spectrum over a wavelength range of 1300-1600 nm.

The constructed prototype of the wavelength reference is an enclosure with a size of 15x10x5 cm connected to a computer via its parallel port. It comprises the etalon inserted in an air gap formed between two fiber-optic collimators, and the electronics needed to temperature stabilize and tune the etalon. The parameters of the wavelength reference can be tuned and monitored with a computer program designed to perform the calculations and to offer an easy-to-use user interface.

We measured the transmission spectrum of the Fabry-Perot silicon etalon described in section 6 over 120 transmission fringes (see Fig. 24). The etalon has 3-layer mirrors. The sharpness of the transmission fringes is characterized by the visibility, which is the ratio between the peak transmission of the etalon and the bottom value in the transmission spectrum. It is seen from Fig. 24 that the visibility of the fringes is largest at wavelengths below 1500 nm and it begins to decrease towards higher wavelengths. This indicates that the thickness of the mirror layers of this etalon is not optimized for the use at wavelengths around 1550 nm. The degradation in the visibility leads to broadening of the transmission fringes, which results in a reduction in the accuracy of the wavelength reference.

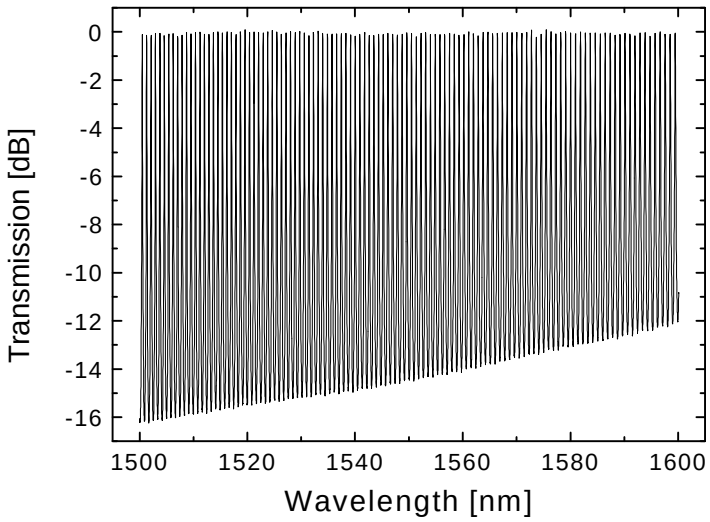


**Figure 24.** Measured transmission spectrum of the Fabry-Perot silicon etalon utilized as a wavelength reference.

### 7.4 Calibration and accuracy of the wavelength reference

The calibration scheme for the etalon includes an initialization in which the relation of all the important parameters is measured once. The reference can then be used without continuous comparison to any external reference. The temperature of the chip can be tuned and monitored with the thin-film resistors and the *FSR* and the position of the transmission fringes can be calculated once the relation between the resistance and the refractive index is calibrated. To measure the accuracy of the etalon-based wavelength reference, one of the transmission fringes is first tuned to the selected wavelength. The position of all of the other transmission peaks are then calculated by applying the information on the temperature of the chip and the wavelength dependence of the refractive index. To estimate the accuracy and the stability of the wavelength reference, beat measurements between a laser stabilized to the peak of a transmission fringe and an acetylene-stabilized laser were performed. The wavelength of a tunable laser (Photonetics Tunics-PRI) was stabilized to the peak of a transmission fringe utilizing lock-in technique as illustrated in Fig. 25 [5]. The laser frequency is sinusoidally modulated and the transmitted intensity through the wavelength reference is detected in phase with the modulation by using a lock-in amplifier. The output of the amplifier is proportional to the first derivative of the transmission signal. The signal crossing serves as the lock point.

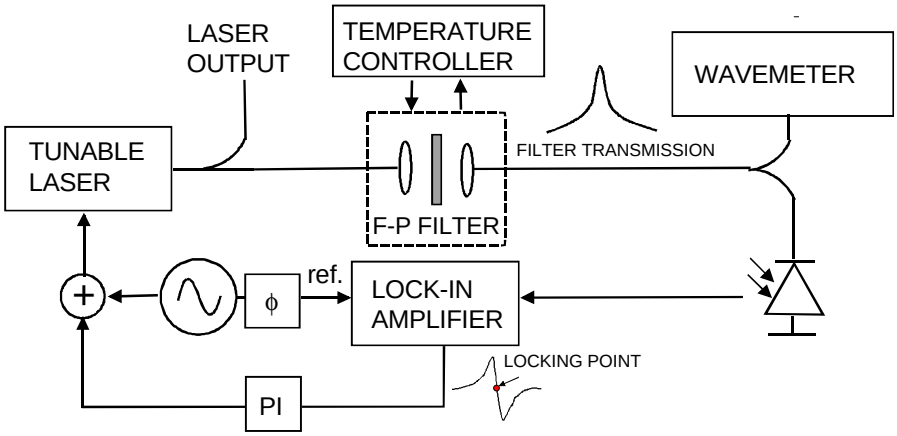


**Figure 25.** A setup for locking the wavelength of a laser to a wavelength reference.

The reference laser was also a tunable laser, which in a similar way was locked to an absorption line of acetylene. The center frequency of the transmission fringe of the etalon was first tuned to a selected frequency close to an absorption line of acetylene. The tuning was accomplished utilizing the numerical model for the refractive index and its temperature dependence. The selected frequency was offset by 700 MHz with respect to the exact value of the absorption line. Any deviation from this nominal value presents an error in the wavelength of the transmission fringe. The accuracy of the wavelength reference was measured against 54 absorption lines in the wavelength region from 1522 nm to 1552 nm. The deviation of the beat signal from its nominal value of 700 MHz for each of the wavelength values is presented in Fig. 26. The deviation is within the range of ± 1 pm (125 MHz) over the whole wavelength range. This accuracy is sufficient for performing the calibrations of the wavelength scale of optical instruments over a wide wavelength range.

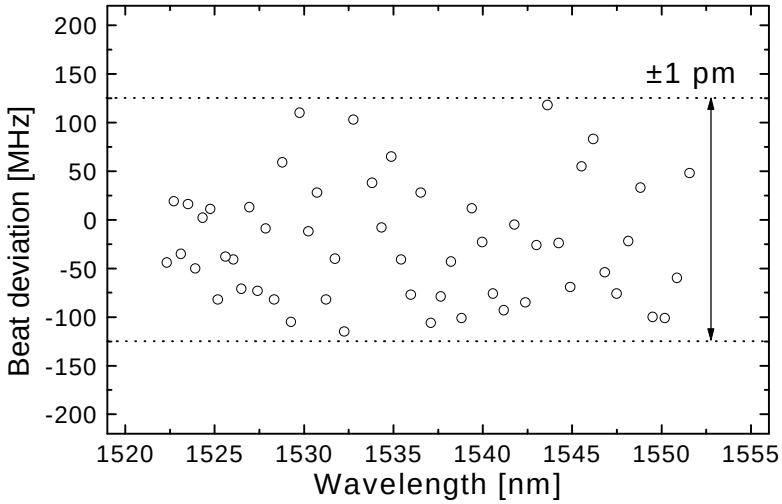


**Figure 26.** Deviation of the beat signal between the acetylene-stabilized reference laser and the laser locked to the etalon-based wavelength reference.

# 8 Summary

Measurement techniques for characterization of various parameters of the key components in modern fiber-optic networks have been investigated. For these purposes, novel filter structures based on temperature-tunable Fabry-Perot etalons were developed. The etalons were fabricated at the Technical Research Center of Finland (Microelectronics) and their cavity material is silicon, which allows for a convenient temperature tuning. Tuning of the temperature was realized with thin-film resistors integrated on the surface of the silicon chip. The main applications of these filters include spectral filtering and wavelength monitoring of optical transmitters and realization of a wavelength reference artifact with an adequate accuracy. Moreover, a novel method for improving the measurement accuracy of the phase-shift method commonly used to determine the dispersion of optical components was developed.

As the bit-rates increase, the influence of dispersion of the optical components such as optical fibers and optical filters becomes more important. It has been pointed out that the results obtained with the conventional phase-shift method might be inaccurate if the group delay of the components fluctuates as a function of wavelength. Such a fluctuation is present for instance in a dispersion-compensating fiber Bragg grating. In this thesis, the performance of the phase-shift method in measuring the group delay ripple was investigated. An instrument function of the operation of the phase-shift method at high modulation frequencies was derived. It was successfully utilized for investigation of the accuracy of the measurement result. By analyzing sinusoidal group delay ripple it was found out that if the applied modulation frequency is more than 1/3 of the period of the ripple, the error in the measured amplitude of the ripple is more than 50 %. Subsequently, a new method to reconstruct the original group delay of the component utilizing the instrument function was developed. Reconstruction of the group-delay was conducted on a dispersion-compensating grating. The new method provides a simple means to improve the accuracy by post-processing the data without any modifications to the measurement setup.

A new device for automated measurements of time-resolved frequency chirp of directly modulated diode lasers was developed. It makes use of a novel temperature-tunable filter as a frequency discriminator. Temperature tuning was realized with two thin-film resistors integrated on the surface of the chip. The chirp analyzer provides an easy solution for analyzing the frequency chirp of the optical transmitters up to the bit-rate of ~10 Gbit/s. The chirp analyzer was further developed to enable measurements of frequency chirp in real time. The real-time chirp analyzer allows for monitoring the frequency chirp as the parameter values such as the bias current or extinction ratio of the laser diode are changed. The time-resolved chirp measurements give fundamental knowledge of the operation of the laser as an optical transmitter. This information about the adiabatic and transient chirp is essential in construction of accurate models used for simulation of the optical transmission systems. Moreover, the analysis of the chirping characteristics can serve as a fast test of the operation of the laser diodes instead of time-consuming bit-error ratio measurements.

Another filter was developed which has high-reflectivity dielectric mirrors on both side of the chip. It was applied in spectral filtering and wavelength monitoring of optical transmitters. The heating and temperature sensing resistors were used to both tune and detect the position of a selected transmission fringe in wavelength. When the transmission of the filter was locked to the slope of the transmission fringe, the variation in the wavelength of the transmitter was monitored by detecting the changes in the resistance of the temperature-

sensing resistor. It was also observed that the extinction ratio of directly modulated transmitters can be increased and their long-haul performance improved. Furthermore, it was confirmed that directly modulated transmitters could be used in long-haul applications with fiber lengths as long as 350 km without any dispersion compensation. This means that by placing this filter inside the laser package both wavelength monitoring and spectral filtering to improve the transmission properties of a directly modulated laser can be performed simultaneously.

The filter was also successfully utilized to reduce the frequency chirp of pulses generated by gain-switching of DFB-lasers. Reduction of the spectral width leads to almost transform limited pulses. However, a series of secondary oscillations were observed after the main pulse when the filter was tuned to induce maximum compression of the width of the pulse. The secondary oscillation could lead to intersymbol interference in optical communications applications.

Moreover, the temperature-tunable Fabry-Perot etalon was employed in realization of a first prototype of a compact and cost-effective wavelength reference. The temperature of the silicon chip was stabilized by utilizing the integrated temperature-sensing resistor in an electronic feedback loop. The Fabry-Perot etalon provides periodic transmission fringes each of which can be used as an accurate wavelength reference provided that the parameters such as the refractive index, the length of the cavity and the temperature coefficient of the refractive index are known. These parameters were accurately determined and a performance adequate for field calibrations was achieved.

In conclusion, measurement methods and applications of a novel temperature tunable optical filter were investigated and several device concepts were successfully demonstrated. The future work with the tunable filter includes fabricating filters with small size to enhance the speed of tuning and packaging of the filter to allow for compact device implementation. The aging effects of the thin-film resistors and the polarization effects induced by the mirror structures should be studied in detail to increase the accuracy of the applications involved with wavelength monitoring.

## References


[1] K. Fukuchi et al., "10.92-Tb/s (273x40-Gb/s) triple-band/ultra-dense WDM optical-repeated transmission experiment", in the *Optical Fiber Communications Conference (OFC'01)*, Anaheim, CA, 2001, PD24-1.

[2] B. E.A. Saleh and M. C. Teich, *Fundamentals of Photonics*, Wiley-Interscience, 1991.

[3] I. H. Malitson, "Interspecimen comparison of the refractive index of fused silica", *Journal of the Optical Society of America*, Vol. 55, No. 10, pp. 1205-1209, 1965.

[4] M. Herzberger and C. D. Salzberg, "Refractive indices of infrared optical materials and colour correction of infrared lenses", *Journal of the Optical Society of America*, Vol. 52, No. 4, pp. 420-427, 1962.

[5] W. Demtröder, *Laser Spectroscopy: Basic Concepts and Instrumentation 2nd ed.*, Springer, Berlin, 1996.

[6] M. Beck, I. A. Walmsley, and J. D. Kafka, "Group delay measurements of optical components near 800 nm", *IEEE Journal of Quantum Electronics*, Vol. 27, No. 8., pp. 2074-2081, 1991.

[7] G. Lenz, B. J. Eggleton, C. R. Giles, C. K. Madsen, and R. E. Slusher, "Dispersive properties of optical filters for WDM systems", *IEEE Journal of Quantum Electronics*, Vol. 34, No. 8, 1998.

[8] M. A. Muriel, A. Carballar, "Phase reconstruction from reflectivity in uniform fiber Bragg gratings", *Optics Letters*, Vol. 22, No. 2, pp. 93-95, 1997.

[9] L. Poladian, "Group-delay reconstruction for fiber Bragg gratings in reflection and transmission", *Optics Letters*, Vol. 22, No. 20, pp. 1571-1573, 1997.

[10] B. Ortega, J. Chapmany, D. Pastor, and M. Ibsen, "Full low-cost characterization of long period superstructure fiber Bragg gratings", *Microwave and Optical Technology Letters*, Vol. 23, No. 4, pp. 255-257,1999.

[11] M. Beck and I. A. Walmsley, "Measurement of group delay with high temporal and spectral resolution", *Optics Letters*, Vol. 15, No. 9, pp. 492-494, 1990.

[12] M. Volanthen, H. Geiger, M. J. Cole, R. I. Laming, and J. P. Dakin, "Low coherence technique to characterize reflectivity and time delay as a function of wavelength within a long fiber grating", *Electronics Letters*, Vol. 32, pp. 757–758, 1996.

[13] S. D. Dyer and K. B. Rochford, "Low-coherence interferometric measurements of fiber Bragg grating dispersion", *Electronics Letters*, Vol. 35, pp.1485–1486, 1999.

[14] E. I. Petermann, J. Skaar, B. E. Sahlgren, R. A. H. Stubbe, and A. T. Friberg, "Characterization of fiber Bragg gratings by use of optical coherence-domain reflectometry", *Journal of Lightwave Technology*, Vol. 17, No. 11, pp. 2371-2378, 1999.

[15] S. Barcelos, M. N. Zervas, R. I. Laming, D. N. Payne, L. Reekie, J. A. Tucknott, R. Kashyap, P. F. McKee, F. Sladen, and B. Wojciechowicz, "High accuracy dispersion measurements of chirped fibre gratings", *Electronics Letters*, Vol. 31, No. 15, pp. 1280-1282, 1995.

[16] Y. O. Noh, D. Y. Kim, S. K. Oh, and U. C. Pack, "Dispersion measurement of a short length optical fiber using Fourier transform spectroscopy", in *Conference on Lasers and Electro Optics (CLEO'99)*, Pacific Rim 1999, paper ThB5, pp. 599-600.

[17] B. Costa, D. Mazzoni, M. Puleo, and E. Vezzoni, "Phase-shift technique for the measurement of chromatic dispersion in optical fibers using LED's", *IEEE Journal of Quantum Electronics*, Vol. 18, No. 10, pp. 1509-1515, 1982.

[18] S. Ryu, Y. Horiuchi, and K. Mochizuki, "Novel chromatic dispersion measurement method over continuous gigahertz tuning range", *Journal of Lightwave Technology*, Vol. 7, pp. 1177–1180, Aug. 1989.

[19] B. Christensen, J. Mark, G. Jacobsen, and E. Bødtker, "Simple dispersion measurement technique with high resolution", *Electronics Letters*, Vol. 29, No. 1, pp. 132-134, 1993.

[20] M. L. Rocha and R. Kashyap, "Characterization of fiber Bragg gratings: A study on accuracy and repeatability", in *Digest of the 4th Optical Fiber Measurement Conference (OFMC'97)*, Teddington, U.K., 1997, pp. 14–17.

[21] D. Derricson (ed.), *Fiber Optic Test and Measurement*, Prentice Hall, New Jersey, 1998.

[22] Chromatic Dispersion Test Solution, 86037C, Agilent Technologies, www.agilent.com.

[23] Optical Network Analyzer, Q7760, Tektronix, www.tektronix.com.

[24] Chromatic dispersion measurement system, CD400L, Perkin-Elmer,

http://opto.perkinelmer.com/

[25] H. Schmuck, "Comparison of optical millimetre-wave system concepts with regarding to chromatic dispersion", *Electronics Letters*, Vol. 31, No. 21, pp. 1848-1849, 1995.

[26] F. Ouellette, "Dispersion cancellation using linearly chirped Bragg grating filters in optical waveguides", *Optics Letters*, Vol. 12, No. 10, pp. 847-849, 1987.

[27] R.I. Laming, W.H. Loh, M. J. Cole, M. N. Zervas, K. E. Ennser, and V. Gusmeeroli, "Fiber gratings for dispersion compensation", in *Conference on Optical Fiber Communication*, OSA Technical Digest Series, Vol. 6 (Optical Society of America, Washington DC, 1997), pp. 234-235.

[28] B. J. Eggleton, A. Ahuja, P. S. Westbrook, J. A. Rogers, P. Kuo, T. N. Nielsen, B. Mikkelsen, "Integrated tunable fiber gratings for dispersion management in high-bit rate systems", *Journal of Lightwave Technology*, Vol. 18, No. 10, pp. 1418-1432, 2000.

[29] K. Enneser, M. Ibsen, M. Durkin, M. N. Zervas, and R. I. Laming, "Influence of nonideal chirped fiber grating characteristics on dispersion cancellation," *IEEE Photonics Technology Letters*, Vol. 10, pp. 1476–1478, Oct. 1998.

[30] Y. Li, D. Way, N. Robinson, and S. Liu, "Impact of dispersion compensation gratings on OC-192 systems", in *Conference on Optical Amplifiers and Their Applications (OAA'98)*, Monterey, CA, 1998, paper TuB5.

[31] T. Niemi, G. Genty, S. Tammela, and H. Ludvigsen, "Fiber grating nonidealities in dispersion compensated CATV links", in *Conference Digest of 5th Optical Fibre Measurement Conference (OFMC'99)*, Nantes, France, September 22-26, 1999, pp. 157-160.

[32] C. Riziotis and M. N. Zervas, "Effect of in-band group delay ripple on WDM filter performance", in *European Conference on Optical Communications 2001 (ECOC'01)*, Amsterdam, Paper Th. M. 1. 3., pp. 492-493.

[33] R. Kashyap and M. L. Rocha, "On the group delay characteristics of chirped fiber Bragg gratings", *Optics Communications*, Vol. 153, pp. 19–22, 1998.

[34] R. Kashyap, *Fiber Bragg Gratings*, San Diego, CA: Academic, 1999.

[35] L. Poladian, "Understanding profile-induced group-delay ripple in Bragg gratings", *Applied Optics*, Vol. 39, pp. 1920–1923, 2000.

[36] C. Clark, M. Farries, K. Visvanatha, and A. Tager, "Measuring chromatic dispersion of fiber gratings", *Lightwave*, vol. 17, pp. 70–77, Feb. 1999.

[37] R. Fortenberry, "Enhanced wavelength resolution chromatic dispersion measurements using fixed sideband technique," in *Conference on Optical Fiber Communication*, OSA Technical Digest Series (Optical Society of America, Washington DC, 2000), TuG8, pp.107–109.

[38] *Gigabit Optical Link Designer (GOLD), Users Manual*, Virtual Photonics Pty. LTD, 1999.

[39] T. Niemi, G. Genty, and H. Ludvigsen, "Group delay measurements using the phase-shift method: Improvement of the accuracy," in *European Conference on Optical Communications 2001 (ECOC'01)*, Amsterdam, Paper Th. M. 1. 5., pp. 496-497.

[40] A. Frenkel and C. Lin, "Angle-tuned etalon filters for optical channel selection in high density wavelength division multiplexed systems", *Journal of Lightwave Technology*, Vol. 7, No. 4, pp. 615-624, 1989.

[41] Y. C. Chung, "Temperature –tuned ZnS etalon filters for WDM systems", *IEEE Photonics Technology Letters*, Vol. 4, No. 6, pp. 600-602, 1992.

[42] G. Cocorullo and I. Rendina, "Thermo-optical modulation at 1.5 *m*m in silicon etalon", *Electronics Letters*, Vol. 28, No. 1, pp. 83-85, 1992.

[43] P. Tayebati, P. D. Wang, D. Vakhshoori, and R. N. Sacks, "Widely tunable Fabry-Perot filter using Ga(Al)As/$AlO_x$ deformable mirrors ," in *Conference on Optical Fiber Communication*, OSA Technical Digest Series, Vol. 2 (Optical Society of America, Washington DC, 1998), pp. 9-10.

[44] C. K. Madsen and J. H. Zhao, *Optical Filter Design and Analysis*, John Wiley & Sons Inc., New York, 1999.

[45] *Properties of Silicon*, Datareviews series No. 4, INSPEC, The Institution of Electrical Engineers, London, 1988.

[46] E. D. Palik (Ed.), *Handbook of Optical Constants of Solids*, Academic Press Inc., New York, 1985.

[47] W. Primak, "Refractive index of silicon", *Applied Optics*, Vol. 10, No. 4, pp. 759-763, 1971.

[48] M. Born and E. Wolf, *Principles of Optics*, 7th ed., Cambridge Univ. Press, Cambridge, 1999.

[49] M. Bertolotti, V. Bogdanov, A. Ferrari, A. Jascow, N, Nazarova, A. Pikhtin, and L. Schirone, "Temperature dependence of the refractive index in semiconductors", *Journal of the Optical Society of America B*, Vol. **7**, No. 6, pp. 918-922, 1990.

[50] M. I. Nathan, W. P. Dumke, G. Burns, F. H. Dill, and G. J. Lasher, "Stimulated emission of radiation from GaAs p-n junctions", *Applied Physics Letters*, Vol. 1, pp. 62, 1962.

[51] R. N. Hall, G. E. Fenner, J. D. Kingsley, T. J. Soltys, and R. O. Carlson, "Coherent Light Emission From GaAs Junctions", *Physical Review Letters*, Vol. 9, No. 9, pp. 366-368, 1962.

[52] T. Miya, Y. Terunuma, T. Hosaka, and T. Miyashita, "Ultimate low-loss single-mode fiber at 1.55 *m*m", *Electronics Letters*, Vol. 15, No. 4, pp. 106-108, 1979.

[53] S. B. Poole, D. N. Payne, R. J. Mears, M. E. Fermann, and R. I. Laming, "Fabrication and characterization of low-loss optical fibers containing rare-earth ions", *Journal of Lightwave Technology*, Vol. 4, No. 7, pp. 870-876, 1986.

[54] R. J Mears, L. Reekie, I. M Jauncey, and D. N. Payne, "Low-noise erbium-doped fibre amplifier operating at 1.54 μm", *Electronics Letters*, Vol. 23, No. 19, pp. 1026-1028, 1987.

[55] G. P. Agrawal and N. Dutta, *Semiconductor Lasers*, 2nd ed., Van Nostrand Reinhold, New York, 1993.

[56] R. S. Tucker, “High-speed modulation of semiconductor lasers”, *Journal of Lightwave Technology*, Vol. LT-3, No. 6, pp. 1180-1192, 1985.

[57] J. C. Cartledge and R. C. Srinivasan, “Extraction of DFB-laser rate equation parameters for system simulation purposes,” *Journal of Lightwave Technology*, Vol. 15, No. 5, pp. 852-860, 1997.

[58] T. L. Koch and J. E. Bowers, “Nature of wavelength chirping in directly modulated semiconductor lasers”, *Electronics Letters*, Vol. 2, No. 25/26, pp. 1038-1039, 1984.

[59] C. H. Henry, “Theory of the linewidth of semiconductor lasers,” *IEEE Journal of Quantum Electronics*, Vol. QE-18, No. 2, pp. 259-264, 1982.

[60] C. H. Henry, “Phase noise in semiconductor lasers”, *Journal of Lightwave Technology*, Vol. 4, No. 3, pp. 298-311, 1986.

[61] M. Osinski and J. Buus, “Linewidth broadening factor in semiconductor lasers - An overview”, *IEEE Journal of Quantum Electronics*, Vol. QE-23, No. 1, pp. 9-29, 1987.

[62] R. A. Linke, “Transient chirping in single-frequency lasers: lightwave system consequences”, *Electronics Letters*, Vol. 20, No. 11, pp. 472-474, 1984.

[63] B. W. Hakki, “Evaluation of transmission characteristics of chirped DFB lasers in dispersive optical fiber,” *Journal of Lightwave Technology*, Vol. 10, No. 7, pp. 964-970, 1992.

[64] J. Wang and K. Peterman, “Small signal analysis for dispersive optical fiber communication systems”, *Journal of Lightwave Technology*, Vol. 10, No. 1, pp. 96-100, 1992.

[65] F. Devaux, Y. Sorel, and J. F. Kerdiles, “Simple measurement of fiber dispersion and of chirp parameter of intensity modulated light emitter”, *Journal of Lightwave Technology*, Vol. 11, No. 12, pp. 1937-1940, 1993.

[66] A. Røysted, L. Bjerkan, D. Myhre, and L. Hafskjær, “Use of optical fibre for characterization of chirp in semiconductor lasers”, *Electronics Letters*, Vol. 30, No. 9, pp. 710-711, 1994.

[67] R. C. Srinivasan and J. C. Cartledge, “On using fiber transfer functions to characterize laser chirp and fiber dispersion,” *IEEE Photonics Technology Letters*, Vol. 7, No. 11, pp. 1327-1329, 1995.

[68] E. Peral, W. K. Marshall, and A. Yariv, “Precise measurement of semiconductor laser chirp using effect of propagation in dispersive fiber and application to simulation of transmission through fiber gratings”, *Journal of Lightwave Technology*, Vol. 16, No. 10, pp. 1874-1880, 1998.

[69] R. A. Linke, “Modulation induced transient chirping in single frequency lasers”, *IEEE Journal of Quantum Electronics*, Vol. 21, No. 6, pp. 593-597, 1985.

[70] C. M. Olsen, H. Izadpanah, and C. Lin, “Time-resolved chirp evaluations of Gbit/s NRZ and gain-switched DFB laser pulses using narrowband Fabry-Perot spectrometer”, *Electronics Letters*, Vol. 25, No. 16, pp. 1018-1019, 1989.

[71] C. M. Olesen, and H. Olesen, “Time-resolving wavelenght chirp with Fabry-Perot etalons and gratings: A theoretical approach”, *Journal of Lightwave Technology*, Vol. 9, No. 4, pp. 436-441, 1991.

[72] M. G. Davis, and R.F. O’Down, “Time-resolved spectral measurements on a multielectrode DFB laser using a Fabry-Perot interferometer,” *IEEE Photonics Technology Letters*, Vol. 6, No. 1, pp. 21-23, 1994.

[73] W. V. Sorin, K. W. Chang, G. A. Conrad, and P. R. Hernday, “Frequency domain analysis of an optical FM discriminator”, *Journal of Lightwave Technology*, Vol. 10, pp. 787-793, 1992.

[74] R. A. Saunders, J. P. King, and I. Hardcastle, “Wideband chirp measurement technique for high bit rate sources”, *Electronics Letters*, Vol. 30, No. 16, pp. 1336-1338, 1994.

[75] B. Christiansen, A. Kyhn, and B. Skjoldstrup, “Time-resolved chirp measurements on optical sources used for G.scs.”, *ITU-Telecommunication Standardization Sector*, Geneve, 27 May - 7 June 1996.

[76] Y. Kotaki, and H. Soda, “Time-resolved chirp measurement of modulator-integrated DFB LD by using a fiber interferometer,” in *Conference on Optical Communication*, OSA Technical Digest Series, Vol. 8 (Optical Society of America, Washington DC, 1995), pp. 310-311.

[77] N. S. Bergano, “Wavelength discriminator method for measuring dynamic chirp in DFB lasers”, *Electronics Letters*, Vol. 24, No. 20, pp. 1296-1297, 1988.

[78] S. Tammela, H. Ludvigsen, T. Kajava, and M. Kaivola, “Time-resolved frequency chirp measurement using a silicon-wafer etalon,” *IEEE Photonics Technology Letters*, Vol. 9, No. 4, pp. 475-477, 1997.

[79] J. Debeau, B. Kowalski, and R. Boittin, “Simple method for the complete characterization of an optical pulse”, *Optics Letters*, Vol. 23, No. 22, pp. 1784-1786, 1998.

[80] B. Kowalski, J. Debeau, and R. Boittin, “A simple and novel method for measuring the chirp parameter of an intensity modulated light source”, *IEEE Photonics Technology Letters*, Vol. 11, No. 6, pp. 700-702, 1999.

[81] R. Trebino, K. W. DeLong, D. N. Fittinghoff, J. N. Sweetser, M. A. Krumbügel, B. A. Richman, and D. J. Kane, “Measuring ultrashort laser pulses in the time-frequency domain using frequency-resolved optical gating”, *Review of Scientific Instruments*, Vol. 68, No. 9, pp. 3277-3295, 1997.

[82] R. Monnard, C. R. Doerr, and C. R. Giles, “Real-time dynamic chirp measurements of optical signal” in *Conference on Optical Fiber Communication*, OSA Technical Digest Series, Vol. 2 (Optical Society of America, Washington DC, 1998), pp. 120-121.

[83] K. Hinton, “Estimating the output field of a directly modulated laser diode”, *IEEE Journal of Quantum Electronics*, Vol. 32, No. 8, pp. 1427-1431, 1996.

[84] P. Hilke, *Transmission of digital television signals in wavelength division multiplexed fiber optic network*, Master’s thesis, Helsinki University of Technology, 2001.

[85] J. C. Cartledge and G. S. Burley, “The effect of laser chirping on lightwave system performance”, *Journal of Lightwave Technology*, Vol. 7, No. 3, pp. 568-573, 1989.

[86] J. C. Cartledge and G. S. Burley, “Chirping-induced waveform distortion in 2.4-Gb/s lightwave transmission systems”, *Journal of Lightwave Technology*, Vol. 8, No. 5, pp. 699-703, 1990.

[87] International Telecommunication Union (ITU), *Recommendation G.957 – Digital transmission systems – Digital sections and digital line system – Digital line systems*, 1998.

[88] K. Hinton and T. Stephens, “Specifying adiabatic lasers for 2.5 Gbit/s, high dispersion IM/DD optical systems”, *Electronics Letters*, Vol. 29, No. 16, pp. 1479-1480, 1993.

[89] P. O. Andersson and K. Åkerman, “Generation of BER floors from laser diode chirp noise”, *Electronics Letters*, Vol. 28, No. 5, pp. 472-473, 1992.

[90] E. E. Bergmann, C. Y. Kuo, and S. Y. Huang, “Dispersion-induced composite second-order distortion at 1.5 μm”, *IEEE Photonics Technology Letters*, Vol. 3, No. 1, pp. 59-61, 1991.

[91] H. A. Blauvelt, N. S. Kwong, P. C. Chen, and I. Ury, “Optimum range for DFB laser chirp for fiber-optic AM video transmission”, *Journal of Lightwave Technology*, Vol. 11, No. 1 pp. 55-59, 1993.

[92] C. H. Lee, S. S. Lee, H. K. Kim, and J. H. Han, “Transmission of directly modulated 2.5 Gb/s signals over 250-km of nondispersion-shifted fiber by using a spectral filtering method”, *IEEE Photonics Technology Letters*, Vol. 8, pp. 1725-1727, 1996.

[93] M. Uusimaa, *Temperature-tunable micro-filter for improving and monitoring transmitter performance in optical communication systems*, Master's thesis, Helsinki University of Technology, 2000.

[94] P. A. Morton, G. E. Shtengel, L. D. Tzeng, R. D. Yadvish, T. Tanbun-Ek, and R. A. Logan, "38.5 km error free transmission at 10 Gbit/s in standard fibre using a low chirp, spectrally filtered, directly modulated 1.55 μm DFB laser", *Electronics Letters*, Vol. 33, pp. 310-311, 1997.

[95] G. E. Shtengel, R. F. Kazarinov, and L. E. Eng, "Simultaneous laser wavelength locking and spectral filtering using fiber Bragg grating", *IEEE 16th International Semiconductor Laser Conference* (ISLC'98), Nara, Japan, October 1998, Paper ThC5, pp. 269 -270.

[96] K. Inoue, "Optical filtering to reduce chirping influence in LD wavelength conversion", *IEEE Photonics Technology Letters*, Vol. 8, pp. 770-772, 1996.

[97] M. McAdams, E. Peral, D. Provenzano, W. K. Marshall, and A. Yariv, "Improved laser modulation response by frequency modulation to amplitude modulation conversion in transmission through a fiber grating", *Applied Physics Letters*, Vol. 71, No. 7, pp. 879-881, 1997.

[98] H. Y. Yu, D. Mahgerefteh, P. S. Cho, and J. Goldhar, "Improved transmission of chirped signals from semiconductor optical devices by pulse reshaping using a fiber Bragg grating filter", *Journal of Lightwave Technology*, Vol. 17, pp. 898-903, 1999.

[99] K. Tamura, E. P. Ippen, and H. A. Haus "Pulse dynamics in stretched-pulse fiber lasers", *Applied Physics Letters*, Vol. 67, No. 2, pp. 158-160, 1995.

[100] L. E. Nelson, D. J. Jones, K. Tamura, H. A. Haus, and E. P. Ippen, "Ultrashort-pulse fiber ring lasers", *Applied Physics B*, Vol. 65, pp. 277-294, 1997.

[101] T. Pfeiffer and G. Veith, "40 GHz pulse generation using a widely tunable all-polarization preserving erbium fiber ring laser", *Electronics Letters*, Vol. 29, No. 21, pp. 1849-1850, 1993.

[102] M. Nazakawa and E. Yoshida,"A 40-GHz 850-fs regeneratively FM mode-locked polarization-maintaining erbium fiber ring laser", *IEEE Photonics Technology Letters*, Vol. 12, No. 12, pp. 1613 –1615, 2000.

[103] H. Ito, H. Yokoyama, S. Murata, and H. Inaba, "Picosecond optical pulse generation from an R.F. modulated AlGaAs D.H. diode laser", *Electronics Letters*, Vol. 15, No. 23, pp. 738-740, 1979.

[104] P. Torphammar and S. T. Eng, "Picosecond pulse generation in semiconductor lasers using resonance oscillation", *Electronics Letters*, Vol. 16, No. 15, pp. 587-589, 1980.

[105] S. Tarucha and K. Otsuka, "Response of semiconductor laser to deep sinusoidal injection current modulation", *IEEE Journal of Quantum Electronics*, Vol. 17, No. 5, pp. 810-816, 1981.

[106] G. J. Aspin and J. E. Carroll, "Gain-switched pulse generation with semiconductor lasers", *IEE Proceedings-I Solid-state and electron devices*, Vol. 129, No. 6, 283-290, 1982.

[107] M. Süleyman Demokan and A. Nacaroðlu, "An analysis of gain-switched semiconductor lasers generating pulse-code-modulated light with a high bit rate", *IEEE Journal of Quantum Electronics*, Vol. 20, No. 9, pp. 1016-1022, 1984.

[108] K. Y. Lau, "Gain-switching of semiconductor injection lasers", *Applied Physics Letters*, Vol. 52, No. 4, pp. 257-259, 1988.

[109] G. P. Agrawal, *Nonlinear Fiber Optics, 2nd ed.*, Academic Press, San Diego, 1995.

[110] L. P. Barry, B. C. Thomsen, J. M. Dudley, and J. D. Harvey, "Characterization of 1.55*m*m pulses from a self-seeded gain-switched Fabry-Perot laser diode using frequency-resolved optical gating", *IEEE Photonics Technology Letters*, Vol. 10, No. 7, pp. 935-937, 1998.

[111] M. Nakazawa, K. Suzuki, and Y. Kimura, "3.2-5 Gb/s, 100 km error-free soliton transmission with erbium amplifiers and repeaters", *IEEE Photonics Technology Letters*, Vol. 2, No. 3, pp. 216-219, 1990.

[112] M. Nakazawa, K. Suzuki, and Y. Kimura, "Generation and transmission of optical solitons in the gigahertz region using a directly modulated distributed feedback laser diode", *Optics Letters*, Vol. 15, No. 10, pp. 588-590, 1990.

[113] M. Nakazawa, K. Suzuki, and Y. Kimura, "Transform-limited pulse generation in the gigahertz region from a gain-switched distributed-feedback laser diode using spectral windowing", *Optics Letters*, Vol. 15, No. 12, pp. 715-717, 1990.

[114] R.T. Hawkings, "Generation of <3 ps optical pulses by fibre compression of gain-switched InGaAs DFB laser diode pulses", *Electronics Letters*, Vol. 26, No. 5, pp. 292-294, 1990.

[115] L. Chusseau and C. Kazmierski, "Optimum linear pulse compression of a gain-switched 1.55*m*m DFB-laser", *IEEE Photonics Technology Letters*, Vol. 6, No. 1, pp. 24-26, 1994.

[116] L. Chusseau, "Propagation of single-mode 1.5-*m*m gain-switched semiconductor laser pulses in normally dispersive fibers", *IEEE Journal of Quantum Electronics*, Vol. 30, No. 11, pp. 2711-2720, 1994.

[117] Y. Matsui, M. D. Pelusi, and A. Suzuki, "Generation of 20-fs optical pulses from a gain-switched laser diode by a four-stage soliton compression technique", *IEEE Photonics Technology Letters*, Vol. 11., No. 10, pp. 1217-1219, 1999.

[118] Y. Katagiri, K. Aida, Y. Tachikawa, S. Nagaoka, H. Abe, and F. Ohira, "High-speed demonstration of wideband synchro-scanned optical disk filter for absolute laser-wavelegth discrimination", *Electronics Letters*, Vol 34, No. 13, pp. 1310-1312, 1998.

[119] H. Nasu, M. Oike, T. Nomura, and A. Kasukawa, "40mW over DFB laser module with integrated wavelength monitor for 50GHz channel spacing DWDM application", in *Proceedings of 27th European Conference on Optical Communications 2001*, Amsterdam, Paper We.P.25, pp. 428-429.

[120] M. Imaki, S. Yamamoto, M. Sato, Y. Nishimura, K. Masuda, S. Takagi, A. Adachi, J. Yamashita, and Y. Hirano, "Wideband athermal wavelength monitor integrated wavelength temperature-tunable DFB-LD module", *Electronics Letters*, Vol. 37, No. 16, pp. 1035-1036, 2001.

[121] S. K. Shin, C.–H. Lee, and Y. C. Chung, "A novel frequency and power monitoring method for WDM network", in *Optical Fiber Communication Conference*, Vol. 2, 1998 OSA Technical Digest Series (Optical Society of America, Washington, D.C., 1998), pp. 168-170.

[122] K. J. Park, S. K. Shin, and Y. C. Chung, "Simple monitoring technique for WDM networks", *Electronics Letters*, Vol. 35, No. 5, pp. 415-417, 1999.

[123] M. Teshima, M. Koga, and K. Sato, "Multiwavelength simultaneous monitoring circuit employing wavelength crossover properties of arrayed-waveguide grating", *Electronics Letters*, Vol. 31, No. 18, pp. 1595-1597, 1995.

[124] T. Niemi, T. Laukkanen, S. Tammela and H. Ludvigsen, "Wavelength monitoring of multi-channel DWDM-systems using a single temperature-tunable Fabry-Perot filter", *in Proceedings of Conference on Lasers and Electro-Optics Europe (CLEO-Europe 00)*, September 10-15, 2000, CtuP4, pp.164.

[125] International Telecommunication Union (ITU), *Recommendation G.692 - Transmission media characteristics – Characteristics of optical components and sub-systems*, 1998.

[126] European Community, 5th Framework GROWTH, generic activity "Measurement and Testing", dedicated call "Certified Reference Materials";
E. G. Grosche, U. Sterr, J. Meissner, D. Humphreys, J. C. Petersen, F. Wonnacott, F. Bertinetto, C. Svelto, R. Lano, and L. Tallone, "Certified reference materials for optical telecommunication wavelengths", in *Conference Digest of 6th Optical Fibre Measurement Conference (OFMC'01)*, Cambridge, UK, September 26-28, 2001, pp. 189-192.

[127] M. Guy, B. Villeneuve, C. Latrasse, and M. Têtu, "Simultaneous absolute frequency control of laser transmitters in both 1.3 *m*m and 1.55 *m*m bands for multiwavelength communication systems", *Journal of Lightwave Technology*, Vol. 14, No. 6, pp. 1136-1143, 1996.

[128] Y. C. Chung and L. W. Stulz, "Synchronized etalon filters for standardizing WDM transmitter laser wavelengths", *IEEE Photonics Technology Letters*, Vol. 5, No. 2, pp. 186-189, 1993.

[129] C. Gamache, M. Têtu, C. Latrasse, N. Cyr, M. A. Dugay, and B. Villeneuve, "An optical frequency scale in exact multiples of 100 GHz for standardization of multifrequency communications", *IEEE Photonics Technology Letters*, Vol. 8, No. 2, pp. 290-292, 1996.

[130] R. Boucher, B. Villeneuve, M. Brenton, and M. Têtu, "Calibrated Fabry-Perot etalon as an absolute frequency reference for OFDM communications", *IEEE Photonics Technology Letters*, Vol. 4, No. 7, pp. 801-804, 1992.

[131] D. A. Humphreys and J. Howes, "Accurate wavelength calibration for optical spectrum analysers using an etalon calibration artifact", in *Digest of the 4th Optical Fiber Measurement Conference (OFMC'97)*, Teddington, U.K., 1997, pp. 72-75.

[132] J. Tuominen, T. Niemi, P. Heimala, and H. Ludvigsen, "Compact Wavelength Reference for Optical Telecommunication Based on a Tunable Silicon Etalon", accepted for an oral presentation in *the 27th triennial General Assembly of the International Union of Radio Science (URSI), Maastricht, The Netherlands, 2002.*

[133] OSA wavelength calibration standard, Item# WCS201, Thorlabs Inc., www.thorlabs.com.

[134] S. L. Gilbert, W. C. Swan, and T. Dennis, "Wavelength control and calibration wavelength division multiplexed optical communication", in Proceedings of the *IEEE International Frequency Control Symposium 2001*, Seattle, US, pp. 122 –126.

[135] T. Dennis, W. C. Swann, and S. L. Gilbert, "Wavelength references for 1300 nm and L-band WDM", ", in *Optical Fiber Communication Conference*, Vol. 3, 2001 OSA Technical Digest Series (Optical Society of America, Washington, D.C., 2001), pp. WDD83-1-WDD83-3.

[136] W. C. Swan and S. L. Gilbert, "Pressure-induced shift and broadening of 1510–1540-nm acetylene wavelength calibration lines", *Journal of Optical Society of America B*, Vol. 17, No. 7, pp. 1263-1270, 2000.

[137] M. Kusaba and J. Henningsen, "The $n_1 + n_3$ and the $n_1 + n_2 + n_4^1 + n_5^{-1}$ combination bands of $^{13}C_2H_2$. Linestrengths, broadening parameters, and pressure shifts", *Journal of Molecular Spectroscopy*, Vol. 209, pp. 216–227, 2001.

[138] K. Nakagava, M. de Labachelerie, Y. Awaji, and M. Kourogi, "Accurate optical frequency atlas of the 1.55-*m*m bands of acetylene", *Journal of Optical Society of America B*, Vol. 13, No. 12, pp. 2708-2714, 1996.

[139] Y. Awaji, K. Nakagawa, M. de Labachelerie, and M. Ohtsu, "Optical frequency measurement of the $H^{12}C^{14}N$ Lamb-dip-stabilized 1.5-*m*m diode laser", *Optics Letters*, Vol. 20, No. 19, pp. 2024-2026, 1995.

[140] M. de Labachelerie, K. Nakagawa, Y. Awaji, and M. Ohtsu, "High-frequency-stability laser at 1.5 *m*m using Doppler-free molecular lines", *Optics Letters*, Vol. 20, No. 6, pp. 572-574, 1995.

[141] M. Poulin, C. Latrasse, N. Cyr, and M. Têtu, “An absolute frequency reference at 192.6 THz (1556 nm) based on a two-photon absorption line of rubidium at 778 nm for WDM communication systems”, *IEEE Photonics Technology Letters*, Vol. 9, No. 12, pp. 1631-1633, 1997.

## Publications

## Publication P1

## Publication P2

## Publication P3

## Publication P4

## Publication P5

## Publication P6